Liquid Structure and Dynamics in the Choline Acetate:Urea 1:2 Deep Eutectic Solvent.

Alessandro Triolo[1,*], Maria Enrica Di Pietro[2], Andrea Mele[2], Fabrizio Lo Celso[1,3], Martin Brehm[4], Valerio Di Lisio[5], Andrea Martinelli[5], Philip Chater[6], and Olga Russina[1,5,*].

[1] Laboratorio Liquidi Ionici, Istituto Struttura della Materia, Consiglio Nazionale delle Ricerche, (ISM-CNR) Rome, Italy

[2] Department of Chemistry, Materials and Chemical Engineering "G. Natta", Politecnico di Milano, Milano, Italy.

[3] Department of Physics and Chemistry, Università di Palermo, Palermo, Italy.

[4] Institut für Chemie, Martin-Luther-Universität Halle–Wittenberg, Halle (Saale), Germany.

[5] Department of Chemistry, University of Rome Sapienza, Rome, Italy.

[6] Diamond House, Harwell Science & Innovation Campus, Diamond Light Source, Ltd., Didcot, Oxfordshire OX11 0DE, UK

Corresponding Authors: A. T. (triolo@ism.cnr.it); O.R. (olga.russina@uniroma1.it)

Abstract.

We report on the thermodynamic, structural and dynamic properties of a recently proposed Deep Eutectic Solvent (DES), formed by choline acetate (ChAc) and urea (U) at the stoichiometric ratio 1:2, hereinafter indicated as ChAc:U. Although the crystalline phase melts at 36-38 °C depending on heating rate, ChAc:U can be easily supercooled at sub-ambient conditions, thus maintaining into the liquid state, with a glass-liquid transition at about -50 °C. Synchrotron high energy X-ray scattering experiments provide the experimental data for supporting a Reverse Monte Carlo analysis to extract structural information at atomistic level. This exploration of ChAc:U's liquid structure reveals the major role played by hydrogen bonding in determining interspecies correlations: both acetate and urea are strong hydrogen bond acceptor sites, while both the choline hydroxyl and urea act as HB donors. All ChAc:U moieties are involved in mutual interactions, with acetate and urea strongly interacting through hydrogen bonding, while choline being involved mostly in van der Waals mediated interactions. Such a structural situation is mirrored by the dynamic evidences obtained by means of ^{1}H NMR techniques, that show how urea and acetate species experience higher translational activation energy than choline, fingerprinting their stronger commitments into the extended hydrogen bonding network established in ChAc:U.

Introduction.

In the last decade large interest has been growing around deep eutectic solvents (DES)[1,2] and their applications in several fields[3–8]. After the classification proposed by Smith et al. of DES in terms of four different types[3], those belonging to type III are among the most commonly encountered ones. These latter DES are composed by a mixture of a salt (e.g. choline (i.e. the (2-hydroxyethyl)-trimethylammonium cation) chloride) with a hydrogen bonding donor (such as urea, glycerol, etc.) with, depending on the concentration ratio between the two components, a melting point depression resulting from their mixing. The large interest on these compounds stems from several appealing properties, not least their cheap production cost and easy preparation and purification. Most of them are also characterised by nonflammability, bio-compatibility and low toxicity, thus turning out to be ideal media for the development of a variety of processes. On the other hand, most of these appealing features stem from the combination of chemical-physical properties of the different components. Accordingly, by (even minor) changes to their chemical nature, one can efficiently modulate the resulting macroscopic performance, thus leading to the classification of DES as task-specific solvents.[4] Among the most well-known DES, we recall the stoichiometric 1:2 mixture of choline chloride (CC) and urea (U), sometimes referred to as reline.[9–16] Dry reline melts at ca. 31 °C[17] and has attracted huge interest over the last few years. Other CC-based DES have been proposed, including CC-glycerol (Gly) 1:2 (glyceline)[18–22], CC-ethylen glycole (EG) 1:2 (ethaline)[22–24] and, more recently, CC-water 1:3.3-4.2 (aquoline)[25–27]. The recent interest in DES stems from the opportunity that they provide to modulate their solvating properties by changes in their chemical composition. Aiming at expanding the spectrum of properties, other anions paired with choline have been explored as well. For example, choline acetate (ChAc) has been recently considered as an interesting ionic liquid to be paired with an HB donor to lead to a DES. ChAc is an ionic liquid with melting point at 51 °C, proposed by Fukaya et al., as an interesting example of an IL composed solely of biomaterials.[28] The opportunity to use it as a salt for preparation of a DES was presented by Zhao et al., who showed the eutectic nature of mixtures of ChAc with urea (1:2), Gly and EG; these DES showed low viscosity, high biodegradability and excellent compatibility with lipase.[29] More recently ChAc mixtures with different HBDs were probed for their efficiency towards enzymatic reaction with β-galactosidase.[30] In 2020, some of us used ChAc-based DES in order to efficiently solubilise hemicellulose at mild conditions. [31]

This intense applicative activity calls for deeper understanding of the chemical-physical properties of ChAc-based DES that have so far received negligible attention compared e.g. to their CC-based equivalents. Here we present a detailed experimental and computational study of structural and dynamic properties of the DES composed by ChAc and urea at 1:2 molar ratio, hereinafter indicated as ChAc:U. The structural properties of ChAc:U have been obtained by merging high-energy X-ray diffraction and a Reverse Monte Carlo computational approach, aiming at extracting atomistic level structural details of the liquid organization in bulk. The sample has also been probed with NMR techniques, aiming at extracting dynamic information related to rotational and translational processes, occurring around room temperature. Overall, this study provides a careful characterization of structural and dynamic properties of a new, eco-sustainable DES, paving the way for its application as a complementary medium to other related DES.

Experimental and Computational details.

Choline acetate (ChAc) used for DSC and X-ray scattering was a TCI product; urea was a Sigma Aldrich product. ChAc and urea were dried under vacuum at ambient temperature for several days. Eutectic mixtures at 1:2 ChAc:U ratio were prepared in a glovebox with an inert atmosphere to reduce ambient moisture contamination, leading to ChAc:U formation (see **Scheme 1**). After mixing, the sealed vials were kept at 40 °C under constant agitation for at least one hour, to lead to a transparent homogeneous liquid. The sample could be maintained amorphous, when kept at ambient temperature (20 °C) in thin sealed capillaries; it would crystallise when kept inside large sealed vials.

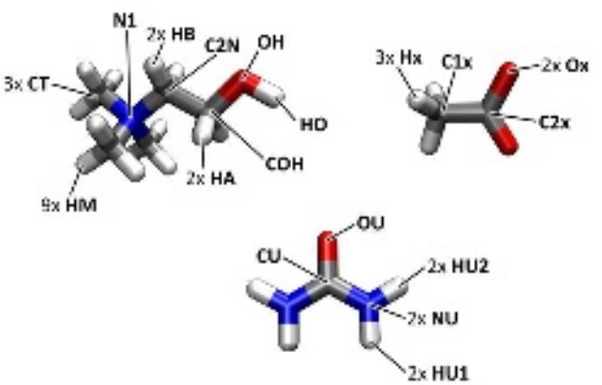

Scheme 1. Schematic representation of choline (top, left), acetate (top, right) and urea (bottom) moieties of ChAc:U (choline acetate:urea=1:2). The nomenclature of the different atomic species is shown.

DSC thermograms were acquired by a Mettler Toledo DSC 822e equipped with a FRS5 sensor and a liquid nitrogen cooler. The furnace was purged during the measurement with dry nitrogen at a flow rate of 30 ml min^{-1}. A sample of about 5 mg was weighted in a 40 µl aluminium pan and rapidly sealed. DSC scans comprised of a cooling from 50 to -125 °C followed by a heating from -125 °C up to 50 °C, with a heating/cooling rate of 2/10 °C min^{-1}.

Warm, liquid ChAc:U was loaded into a borosilicate capillary of 1.5 mm outer diameter, which was glue-sealed. After this operation, the sample maintained liquid even at ambient temperature (ca. 20°C). The total high-resolution X-ray scattering data were collected on the I15-1 beamline at Diamond Light Source, UK, using X-rays of wavelength 0.309574 Å and a Perkin Elmer XRD 4343 CT detector. The total scattering data were integrated to 1D using DAWN[32] and then normalised and corrected to extract S(Q) using GudrunX[33,34].

ChAc and U for NMR experiments were purchased from Iolitec and Sigma Aldrich, respectively, and used without further purification. The DES at 1:2 molar ratio was prepared by the heating method, by mixing the two constituents at 80 °C under stirring for 1h, until a homogeneous and transparent liquid was formed. As the freshly prepared ChAc:U nor its starting components were dried, a residual amount

of water is present in the sample (5.7 wt% by Karl Fischer titration). Controlled amounts of water are beneficial to reduce the viscosity and allow for satisfactorily resolved NMR spectra. The sample was transferred to a 5 mm NMR tube, equipped with a capillary containing DMSO-d_6. NMR measurements were performed at 11.74 T NMR with a Bruker NEO 500 console equipped with a direct observe BBFO (broadband including fluorine) iProbe (^{1}H resonance frequency of 500.13 MHz). Measurements were performed over a temperature range of 278 K to 358 K, in 5 K increments, and a minimum of 15 min allowed for thermal equilibration. The residual amount of water together with the liquid tendency to remain in a supercooled state when slowly cooled (see Results & discussion) allowed for NMR measurements at such temperatures.

T_1 relaxation measurements were carried out without sample spinning with the inversion recovery (IR) pulse sequence, using relaxation delays at least five times the longest T_1, and the instrument was carefully tuned, shimmed, and the 90° pulses calibrated before each measurement. The spin−lattice relaxation rates were measured using data matrices of 16384 (t_2) × 16 (t_1), over a spectral width of 9 ppm for various delay times τ, ranging from 0.05−5 to 0.05−12 s, according to the temperature. A total of two transients per increment were collected for each T_1 experiment. The baselines of all arrayed T_1 spectra were corrected prior to processing the data and integrals were used to calculate relaxation times. A single exponential decay was observed for all samples over the entire temperature range investigated. Relaxation times were computed from experimental raw data by means of the Bruker T_1/T_2 relaxation module using the manual integration option and applying the standard one-component fitting function. Data were processed three times and errors were calculated from the maximum standard deviation found at the lowest temperature. Maximum errors are estimated to be 1%. Fits to extract the correlation times and rotational activation energies from the relaxation rates were performed with OriginPro 2018 using a user-defined function with the Levenberg–Marquardt algorithm. For the fit procedure, average errors were estimated to be 5%

Self-diffusion coefficients were measured by pulsed field gradient (PFG) experiments by applying sine-shaped pulsed magnetic field gradients along the z-direction up to a maximum strength of G = 53.5 G cm^{-1}. All the diffusion experiments were performed using the bipolar pulse longitudinal eddy current delay (BPP-LED) pulse sequence. All experiments were carried out over a spectral width of 9 ppm, with a total of eight transients per increment. The relaxation delay was set to at least five times T_1, and four dummy scans were programmed prior to acquisition. The pulse gradients were incremented from 2

to 95% of the maximum gradient strength in a linear ramp with 32 steps. For each DOSY experiment, the duration of the magnetic field pulse gradients (δ) and the diffusion times (Δ) were optimized to obtain, where possible, 95% signal attenuation for the slowest diffusion species at the last step experiment. δ values were in the 2.4−6 ms range, while Δ values were 0.4−0.8 s long. The baselines of all arrayed spectra were corrected prior to processing the data. Data were processed using an exponential filter in F2 dimension (LB = 0.3 Hz), and integrals were used in calculating relaxation times. The determination of self-diffusion coefficients used the Bruker T_1/T_2 module of TopSpin for each peak. The precision of the measured diffusion coefficients is estimated to be within 3%.

2D ^{1}H-^{1}H nuclear Overhauser enhancement (NOESY) experiments were recorded at 298 K by using the phase-sensitive ge-2D NOESY pulse sequence using echo-antiecho (noesyetgp in the Bruker library). Spectra were recorded using eight transients over 4096 (t_2) × 256 (t_1) complex data points. 32 dummy scans and mixing times in the range 20 – 500 ms were used. The relaxation delay was set to 4 s. The NOESY data sets were processed by applying a sine squared window function in both dimensions (SSB = 2) prior to the Fourier transform.

The EPSR approach has been used to model the X-ray diffraction data.[35] This is a robust Reverse Monte Carlo approach (using a NVT ensemble) that is based on the optimization of the empirically proposed potential that leads to the best agreement with experimental diffraction data.

We used a simulation box containing 100 ChAc ion pairs and 200 urea moieties (ChAc:Urea=1:2) with a density of 1.17 g/cc[30] (cubic box size=35.3 Å) at 25 °C. The starting interatomic potential used for choline and urea is the one that was successfully used by Hammond et al. in their study of reline.[10,36] The acetate interaction potential parameters are the same used by Bowron et al. in their study of acetate based ionic liquids.[37] The used parameters are reported in the Supplementary Information. After an equilibration of ca. 6,000 steps, the EPSR was activated and further 10,000 steps delivered a good agreement of the calculated diffraction pattern with the experimental one. At this stage, further 7,000 steps were collected to achieve statistical accuracy on the structural observables (pair distribution functions, angular distributions etc.). In order to evaluate structural properties from the resulting Monte Carlo trajectories, the TRAVIS software was used.[38–40]

Results & discussion.

ChAc:U's DSC trace is shown in **Figure 1**, where two thermal traces are shown with heating/cooling rates equal to 2 and 10°C/min, respectively. It appears that ChAc:U, if cooled from the melt state, can be easily supercooled, maintaining in the liquid state and eventually converting into a glass, without crystallization intervening. The liquid-glass transition (Tg) can be detected in a small temperature range between -48 and -50 °C in both cooling and heating stages. On the other hand, upon heating the glass, cold-crystallization (Tcc) occurs at 6 °C and 19 °C depending on the heating rate. Soon after, the crystalline phase of ChAc:U melts at Tm = 36 °C at 2°C/min or at Tm = 38 °C at 10 °C/min.

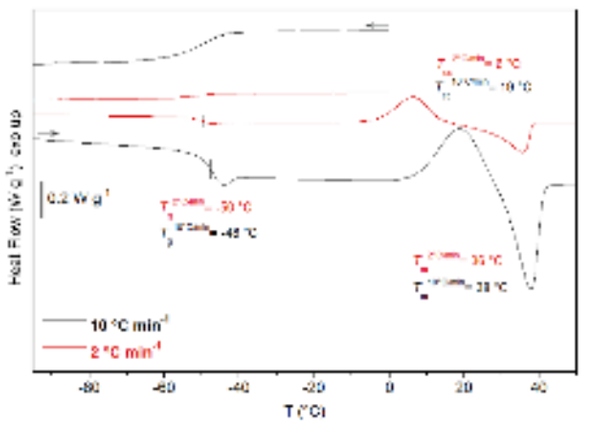

Figure 1. Thermal traces of ChAc:U recorded at two different heating/cooling rates (2 and 10 °C min^{-1}, respectively). Indications of the liquid-glass transition (Tg), cold-crystallization (Tcc) and crystal melting (Tm) are highlighted.

It is noteworthy that, upon cooling from the melt, ChAc:U remains in the liquid supercooled state at 20 °C for long time (several days). Accordingly, we determined the liquid structure of ChAc:U at ambient temperature, without incurring into sample crystallization during the experiment time duration. Synchrotron X-ray diffraction data collected in such a way are reported in **Figure 2**. It appears that ChAc:U is characterised by an X-ray diffraction pattern similar to the ones from other choline-based DES, such as reline, aquoline etc. [10,11,21,24,27,41–43]

The quality of the agreement of experimental X-ray scattering pattern and the corresponding EPSR computed quantity is shown in **Figure 2**. The EPSR-derived X-ray weighted scattering pattern nicely accounts for the experimentally observed features, thus providing a validation support to the structural information that can be extracted from the computed trajectories. It can be appreciated that similarly to other choline-based DES[10,11,21,24,27,41–43], the experimental X-ray scattering pattern does not show appreciable features at low Q values, apart from the low Q peak at ca. 1.5 $Å^{-1}$, thus suggesting that no large scale structural heterogeneities occur in this system, which could be related either to polar/apolar

segregation [44–47] or to mesoscopic phase separation[48–50]. The EPSR-generated trajectories were further interrogated to extract structural information on bulk ChAc:U.

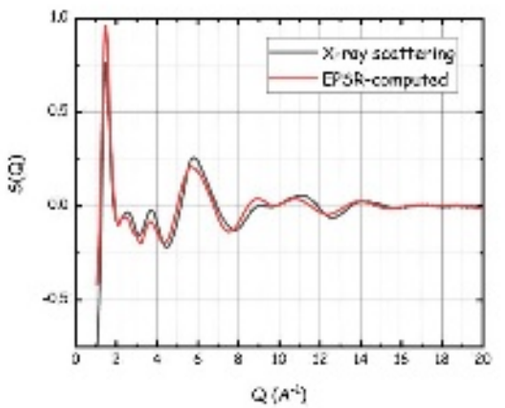

Figure 2. Comparison between experimental (black) and EPSR-computed (red) X-ray scattering patterns from ChAc:U at ambient temperature.

Figures 3 shows the center of mass pair distributions functions (pdf) for the three moieties in ChAc:U, namely, choline cation (C), acetate anion (A) and urea (U). It emerges that strong correlations exist between differently charged ionic species and between urea and all the components. Correlations between ionic species with the same charge are instead weaker and less well defined. CC correlations are characterised by a weak broad peak centred at ca. 6.5 Å, building up a solvation shell containing ca. 3 moieties. This coordination number is substantially different from what is found in the case of reline,

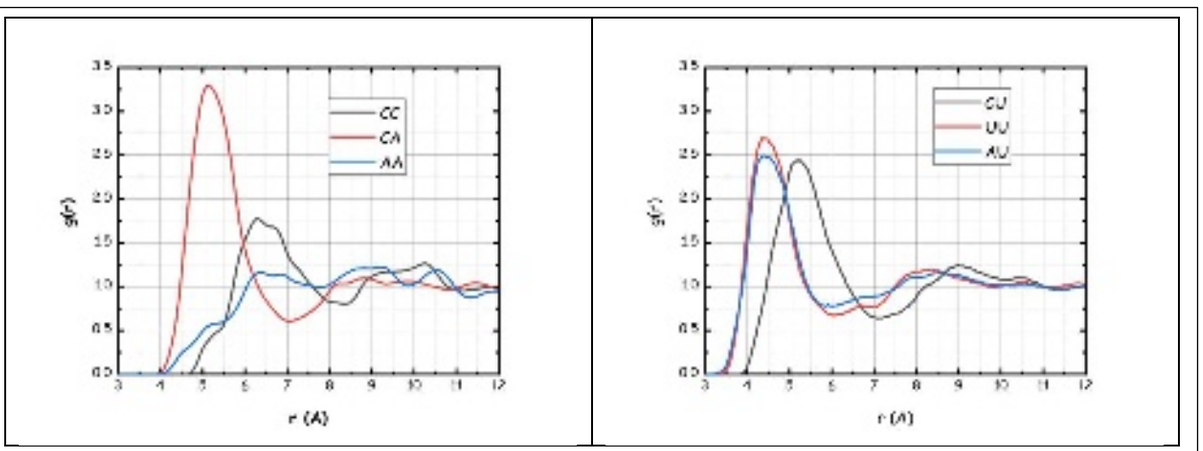

Figure 3. Pair distribution function between centers of mass of ionic species (cation (C), anion (A)) (left) and urea (U) with A and C (right) in ChAc:U, as obtained from the EPSR modelling.

where choline is surrounded by approx. 6 other choline cations. Such a situation likely stems from the larger size, as well as the different shape and symmetry of acetate as compared to chloride anions. Each choline cation is on average surrounded by 3.4 acetate anions with a correlation peak at 5.3 Å. For comparison in reline, 4.5 chloride anions where found in the first shell[10], while 1 chloride anion was found in the same shell in malicine[51]. Urea is characterised by strong correlations both with other urea moieties and with both cations and anions. First solvation shells are detected around each ionic species, with peaks centred at 5.1 Å and 4.5 Å and 6 and 4 nearest neighbour urea moieties for choline and acetate, respectively.

Figure 4 reports a series of pdfs related to selected correlations between atomic species belonging to the different moieties building up bulk ChAc:U.

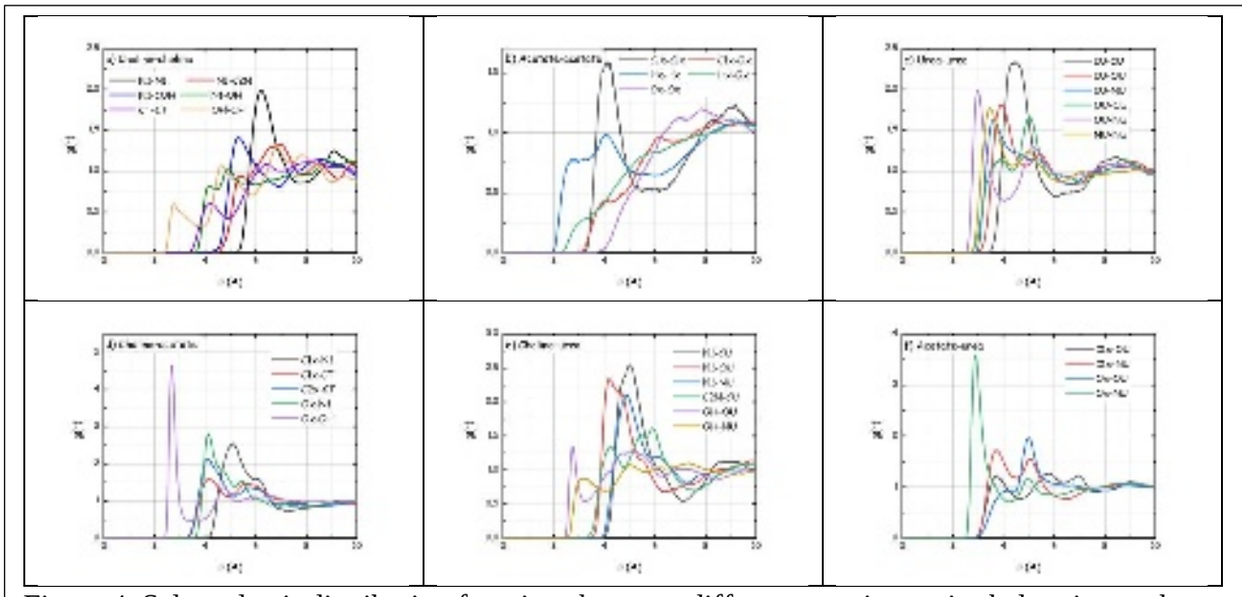

Figure 4. Selected pair distribution functions between different atomic species belonging to the three moieties in ChAc:U (choline, acetate and urea, respectively), after the EPSR modelling.

The selected pdfs indicate the existence of strong correlations between the different moieties. In particular, those pdfs involving acetate and either choline or urea, are characterised by strong peaks, fingerprinting hydrogen-bonding mediated interactions. Such interactions will be further explored later in the manuscript. Choline-choline correlations are rather weak and broadly distributed. The strongest correlation is between neighbour nitrogen atoms, with a peak centred at 6.5 Å, and a neighbour number of ca. 2.5 up to 7 Å. We also detect a relatively strong N1-COH correlation centred at ca. 5.3 Å with approximately 2.5 nearest neighbours (n.n.); however there is only weak interaction of the nitrogen

with the hydroxyl group (weak peaks for N1-OH between 4 and 5 Å). Neighbour acetate anions are only correlated through their methyl groups for which we detect a C1x-C1x peak at 4 Å, with one methyl group directly correlated to the reference one. Urea-urea correlations look more structured: we will see later that this is also because of the existence of hydrogen bonding interactions and accordingly we find strong peak in the OU-NU pdf at ca. 3 Å, with a n.n. population of 2 NUs around the reference OU. The other peaks reported in **Figure 4 c)** indicate the existence of strong correlations also between other urea's moieties such as NU-NU (3 n.n.), CU-OU (2 n.n.) and, in particular, CU-CU (4 n.n.). Similar observations led Edler et al. to propose the existence of urea clustering in reline.[10] Inter-species correlations are dominated, as we will see later in more detail, by HB correlations. Overall these correlations look much stronger than correlations between similar species. The selected pdfs in **Figures 4 d)-f)** reflect in an indirect way the existence of such interactions. Choline-acetate correlations are characterised by a strong Ox-OH peak at 2.7 Å, fingerprinting the HB between the two species. The broad peak related to the Cation-Anion pdf in **Figure 3** is likely related to the existence of different solvation scenarios of acetate around the reference choline: in particular, acetate will coordinate choline both at the hydroxyl side and at the ammonium side. This latter scenario is fingerprinted in the Ox-N1 and C1x-N1 pdfs by the strong peaks centred at 4.2 and 5 Å, respectively. Choline and urea appear to interact mostly through choline's ammonium: pdf peaks for N1 with CU, NU and OU are eminent at distances between 4 and 5.5 Å. Correlations mediated through choline's hydroxyl group look weaker. The competition between acetate and urea in coordinating choline's N1 leads to ca. 5 urea and 3 acetate moieties surrounding N1 by a distance of ca. 7 Å. For comparison, the OH moiety of choline is solvated by 0.6 acetate and 0.9 urea in the first shell (up to 4.5 Å) and ca. 2 choline in the first shell (up to 7 Å). Acetate and urea interact through HB involving urea's hydrogen and the carboxyl group; such an interaction, fingerprinted by the Ox-NU peak at ca 3 Å, is consistent with two different solvation environments indicated by the two peaks in the C1x-NU pdf (3.7 and 5 Å).

As mentioned, HB interactions are fundamental in driving structural correlations in ChAc:U. In **Figure 5**, the pair distribution functions associated to such correlations involving either the choline HOH or the urea HU1/2 donor groups. In particular, we specifically monitor the two hydrogens, HU1 and HU2, attached to the same nitrogen in urea (HU1 being the hydrogens in trans with the urea's oxygen and HU2 being the cis hydrogens), aiming at assessing differences in the HB features, due to steric hindrance. For these HB correlations the combined distribution functions accounting for the distance H··O and the angle D-H··O (where D is the HB donor atom) are reported in the supplementary

262 information (**Figures S1-3**). In all cases, HB involving the acetate HB acceptor (Ox) are characterised

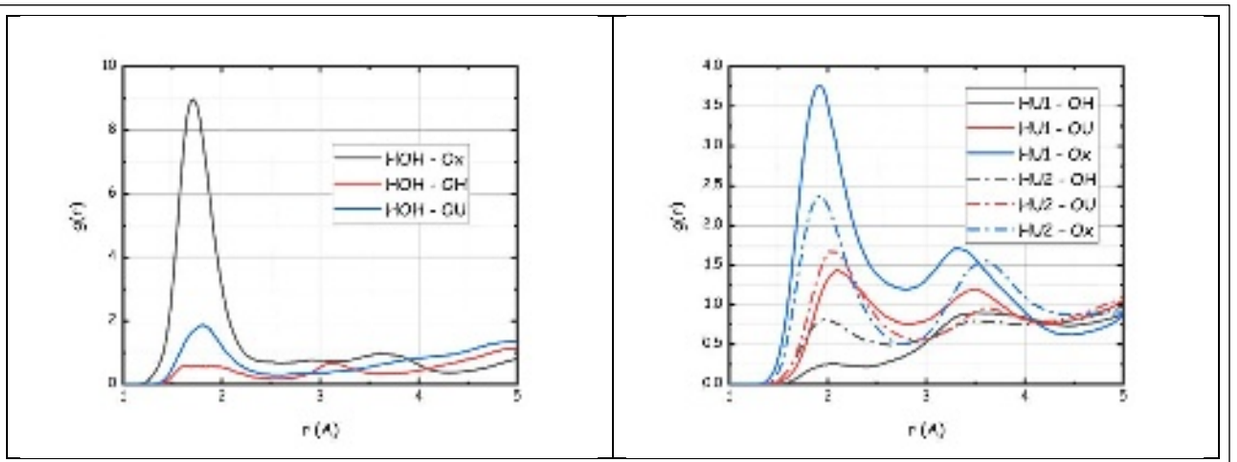

Figure 5. Pair distribution functions related to hydrogen bonding interactions in ChAc:U, as obtained from the EPSR modelling: (left) pdf related to the HOH donor agent in choline and (right) pdf related to the trans (HU1) and cis (HU2) hydrogens in urea.

263 by the shortest and strongest interaction, also the angular dependence of these HB reflects their
264 linearity. In terms of pdf peak amplitude, the next most intense peaks correspond to those involving
265 urea's oxygen (OU) and finally choline's oxygen (OH). Overall, all these HB interactions are found to be characterised by a quite linear geometry, as shown in Figures **Figures S1-3.** In order to better illustrate the balance between HB donor and acceptor capabilities of the different moieties in ChAc:U, we exploit the linear Sankey diagram approach of **Figure 6**, introduced recently for this kind of analysis.[39] A wealth of information can be straightforwardly extracted from such a plot, on the nature of HB networking in ChAc:U. The hydrogen bond donated by choline OH (HOH) (upper left) is mainly involved with the acetate Ox (lower right). There is only a tiny amount of hydrogen bonding interaction between HOH and choline OH and negligible interaction with urea. The trans and cis protons of urea (HU1

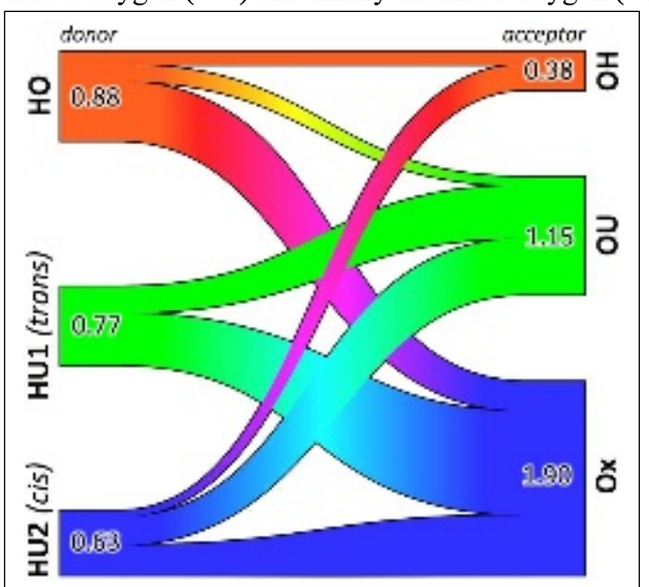

Figure 6. Linear Sankey diagram describing the hydrogen bonding topology in ChAc:U. Numbers correspond to the average hydrogen bond count per donor/acceptor.

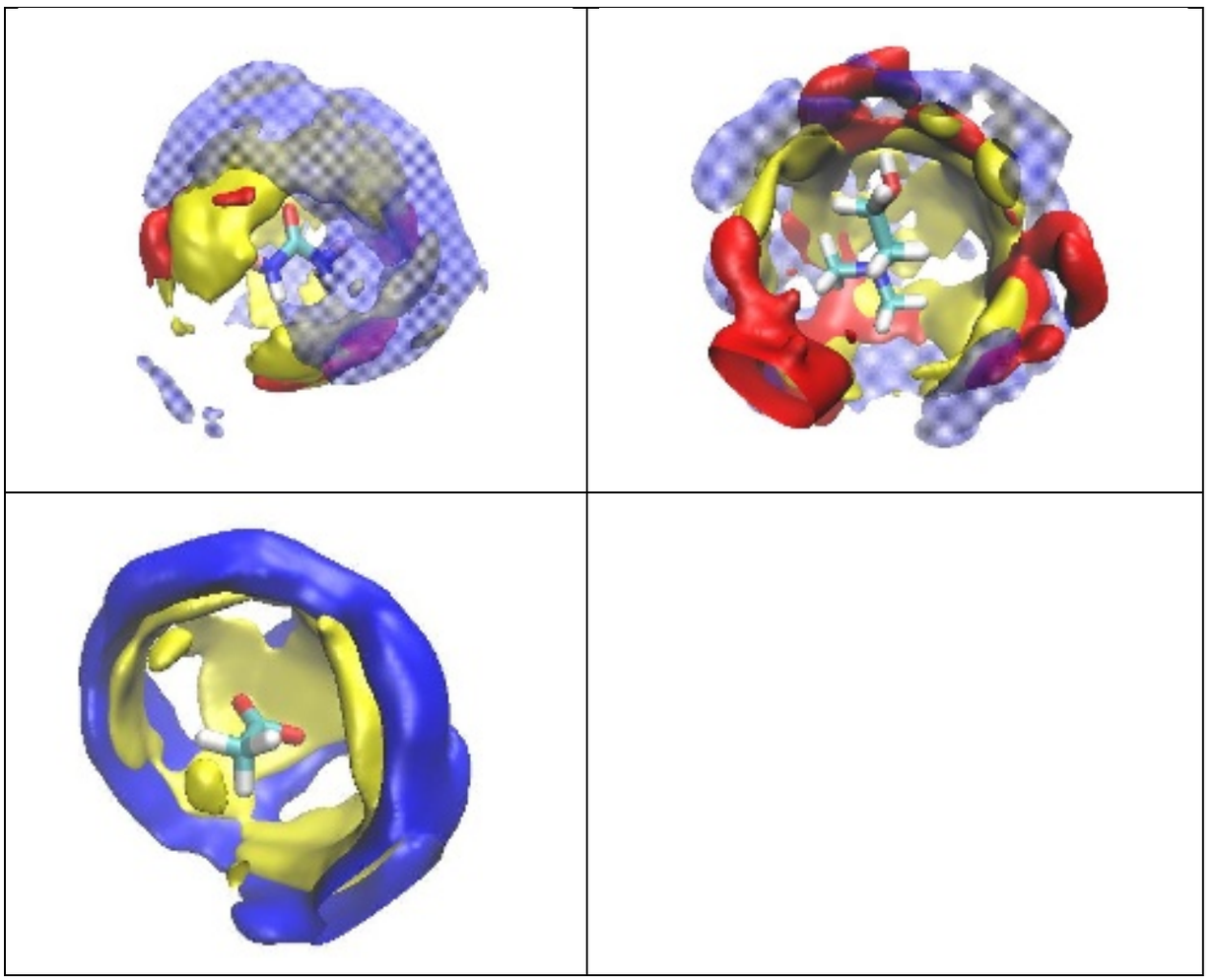

Figure 7. Spatial distribution functions around reference urea (top, left), choline (top, right) and acetate (bottom, left). The coloured lobes correspond to 20% distribution of choline (blue), acetate (red) and urea (yellow) in ChAc:U.

and HU2, respectively) behave differently. While the trans protons (HU1, middle left) do not form hydrogen bonds to choline OH, but form strong hydrogen bonds to both urea OU and acetate Ox, the cis protons (HU2, lower left) also form hydrogen bonds with choline OH. Now considering the acceptors (right side), incoming hydrogen bonds at choline OH almost exclusively come from the urea cis protons, HU2. The urea oxygen receives strong hydrogen bonds from both cis and trans urea's protons, while it almost receives no hydrogen bonds from choline HOH. A similar picture arises for acetate Ox, where the hydrogen bond received from the urea trans protons is most significant. Overall,

the major role played by the acetate anion in establishing HB interactions is confirmed by this graph; analogously the minor role played by choline's OH acceptor site is also highlighted.

Additional understanding of the mutual spatial distribution of the different species with respect to each other can be obtained by inspecting the spatial distribution functions reported in **Figures 7.** The first of such plots refers to the distribution of the three different moieties surrounding a reference urea molecule. Urea is strongly correlated with acetate anions (red lobes) at spatial locations corresponding to its cis and trans hydrogens. Choline cations (blue lobes) distribute in a much more homogeneous way around urea and correlations are not driven by HB, but rather by dispersive interactions. Finally, urea (yellow lobes) competes with acetate to access the reference urea hydrogens; it moreover interacts with reference urea oxygen. It also appears that choline tends to distribute around urea, aiming at interacting also with the other species surrounding the reference one. In **Figure 7** the distributions around a reference choline cation are also shown. The acetate anion is strongly interacting with the hydroxyl group, with a weak competition on this site with urea; otherwise, both the choline cation and urea are distributed rather homogeneously around the whole reference choline, with urea approaching closer than choline the reference molecule. **Figure 7** also shows the distributions of cations and urea around a reference acetate anion. The two species have similar distributions, although urea succeeds in accessing closer to the anion, presumably due to its smaller size. Both moieties approach the anion from the charged carboxyl part, thus reflecting the development of hydrogen bonding interactions. Anions tend to approach the reference acetate from the opposite side, leading to methyl-methyl group correlations (data not shown).

These pictures are consistent with the overwhelming role played by acetate in HB interacting with both urea's and choline' HB donor hydrogens. On the other hand, the HB donor and acceptor nature of urea and the possibility of choline to interact not only with coulombic forces, but also with dispersive ones, make these two moieties able to efficiently solvate any component in ChAc:U. Analogously to the case of reline, an intertwining of the different species occurs in delivering an intimate mixing of these components at atomic level.

To corroborate the structural picture emerging from the combined X-ray / Reverse Monte Carlo approach, variable-temperature NMR measurements were performed. As inter-species correlations appear to be dominated by HB interactions, the upfield or downfield movement of the temperature-dependent ^{1}H chemical shift was monitored to give a preliminary insight into the strength of the HB of the detected proton. **Figure 8** shows the relative shifts of the ^{1}H NMR signals of ChAc:U, which are defined as $\Delta\delta = \delta - \delta_0$, with δ_0 the chemical shift of a given proton in the pure DES and δ the chemical shift of the same proton for increased temperature. [52,53]

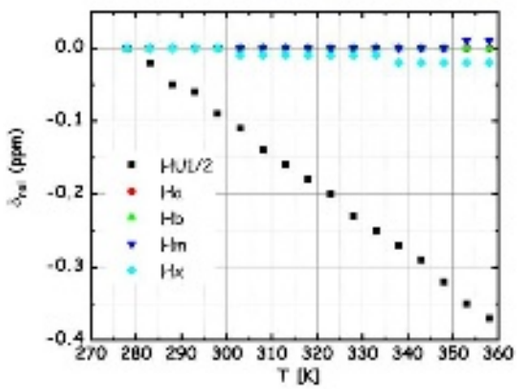

Figure 8. ^{1}H relative shift observed for ChAc:U as a function of the temperature.

The remarkable upfield shift of urea protons is compatible with a weakening of the H-bond strength at the urea site with temperature,[54] and points towards their strong involvement in the HB network of the mixture. No relevant changes are observed for the choline signals, including the N-methyl groups, which is in line with a minor role played by the cation in the intermolecular network. Only a tiny upfield shift emerges for the methyl group of acetate, as they do not directly participate in the HB interactions but most likely feel a pale indirect effect of the major role played by the acidic group of the anion.

The NMR experiments of choice to probe spatial intermolecular networks are typically based on the nuclear Overhauser enhancement (nOe). In extensively connected systems like DES it is however quite common to observe intra- and inter-correlations between all sites/species in the mixtures.[55,56] This is the case for ChAc:U too, as displayed in **Figure S4** in the Supporting Information. Due to spin diffusion and/or exchange (facilitated by the residual water), all signals are positive. Choline shows intramolecular NOE signals, and intermolecular NOE are observed between all the three species, choline, acetate and urea. As expected, intense correlations are observed between the hydroxyl group proton of choline and urea, and the N-methyl groups of choline and urea. The methyl group of acetate shows the strongest correlations with the N-methyl protons of choline and with urea. This confirms the major role of these protons in the interactions holding the DES components together.

The NOESY data provide then support to the scenario of an extended HB network in the DES, which is the root of its peculiar macroscopic properties. We also exploited relaxation and diffusion NMR experiments to shed more light on the system. Intermolecular interactions and dynamics are indeed intertwined, as strong correlations reduce motion – as one can intuitively envisage. T_1 relaxation times and self-diffusion coefficients were measured over an 80 °C temperature interval and analyzed to get quantitative descriptors of the motion(s).

As displayed in **Figure S5** in the Supporting Information, all temperature-dependent T_1 curves, but that corresponding to methyl protons of acetate, pass through a minimum. This indicates that the protons of choline and urea undergo a transition from the extreme narrowing ($\omega_0\tau_C < 1$) to the diffusion limit ($\omega_0\tau_C > 1$) relaxation regime between ~25 °C and ~50 °C. Contrarily, the methyl protons of the anion fail to undergo this transition in the studied temperature range due to their higher mobility. In the case of ^{1}H T_1, where the predominant relaxation mechanism is the homonuclear dipole−dipole interaction, the relaxation rate R_1 is defined by the Bloembergen, Purcell, and Pound (BPP) approach as:[57–59]

$$R_1 = \frac{1}{T_1} = C\left(\frac{\tau_C}{1+\omega_0^2\tau_C^2} + \frac{4\tau_C}{1+4\omega_0^2\tau_C^2}\right) \quad (1)$$

with ω_0 the observe frequency (rad s^{-1}) and C a term evaluated separately for each nucleus. The correlation time of the dipolar interaction τ_C can be thought of as the time required for the vector connecting the interacting nuclei to rotate through the angle of one radian, and for small rigid molecules it commonly reflects the molecular reorientational time constant.[59] As for flexible ionic liquids[60,61], the τ_C observed for ChAc:U have to be rather considered as a combination of molecular reorientation and internal motions of each given segment. From the term in brackets in Eq. (1), it follows that T_1 is minimum when $\omega_0\tau_C = 2\pi\nu_0\tau_C = 0.616$ [61–63], which means here $\tau_C = 0.616/(2\pi \cdot 500.13 \cdot 10^6 \text{ Hz}) = 196$ ps. Such minimum T_1 value can be used to calculate C from Eq. (1), then enabling the calculations of τ_C values from the T_1 values observed at any temperature. The temperature-dependent correlation times can be then used in an Arrhenius-type equation to calculate the "apparent" activation energy E_a^{rot} (averaged over several types of movements).[61,64] Alternatively, by substituting the function of the correlation time approximated as an Arrhenius expression into the BPP equation (Eq. (1)), and assuming C temperature insensitive, the combined equation can be directly solved yielding the same outputs within the experimental error. [61,65] Although the two methods are essentially the same from the theoretical standpoint, the latter nonlinear least squares method is useful

in cases where an exact minimum is not reached in the examined temperature range, and is recommended even for protons where a T_1 minimum can be distinctly observed as it needs less steps with a reduced margin of error.[61] The nonlinear least squares method was used here to fit all T_1 data obtaining the correlation times and activation energies reported in **Figure 9**. All temperature-dependent curves followed perfectly the BPP model, which means that a single basic motion occurs in the studied temperature range.[62] The best-fit parameters are given in **Table S1** in the Supporting Information, together with those obtained by applying the most widely used method based on the T_1 minimum followed by Arrhenius plot of the activation energies, to confirm that comparable results are obtained. Urea protons show the longest τ_C values (slowest rotational motion), and the methyl protons of acetate the shortest ones (fastest rotational motion), while the three methylene and methyl sites of choline

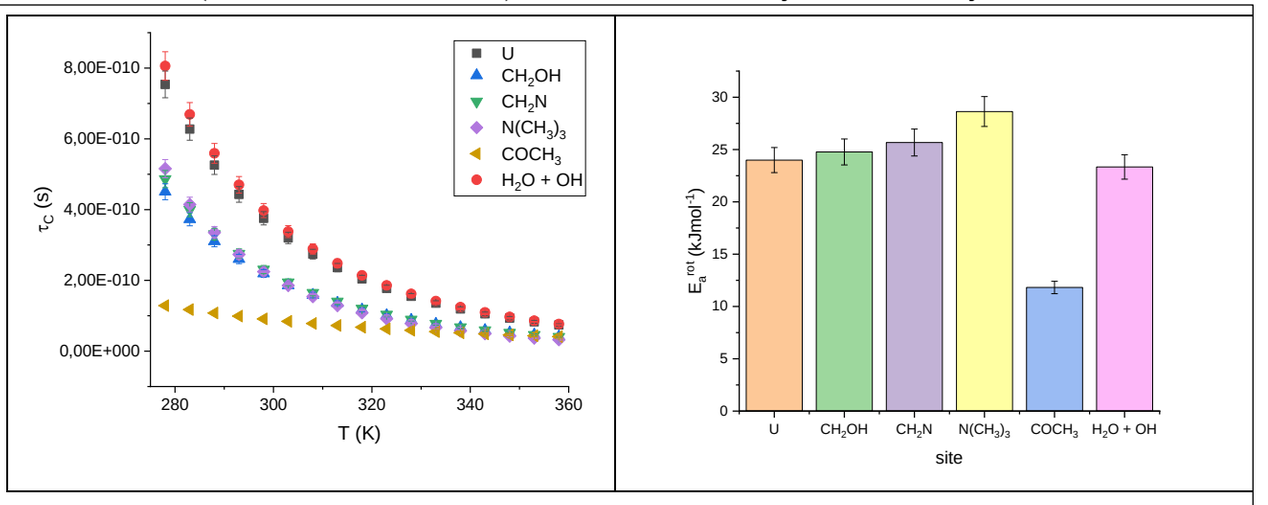

Figure 9. (left) ^{1}H correlation times τ_C vs temperature and (right) rotational activation energy E_a^{rot} (kJ mol^{-1}) obtained for the different proton sites of ChAc:U.

exhibited all close, intermediate τ_C values. A direct comparison between the correlation times of the different sites and species is complicated due to the contribution of different relaxation mechanisms. More informative are the rotational activation energies, which mark a significant difference between acetate from the one side, with E_a^{rot} of ca. 12 kJ mol^{-1}, and choline and urea from the other, all with E_a^{rot} above 20 kJ mol^{-1}. Hence, the rotational motion of the acetate protons is not only the fastest, also due to the intramolecular rotation around the symmetry axis of the methyl group, but it also requires less energy to occur. For the sake of completeness, we also report the correlation times and rotational activation energy obtained from the BPP analysis of the temperature-dependent T_1 data of the peak corresponding to the residual water and the hydroxyl proton of choline (**Figures S5 and 9**). All T_1, τ_C

and E_a^{rot} values essentially overlap those corresponding to urea protons, pointing towards a strong correlation between the rotational motion of the two species. Despite its relevance, the role of water in the intermolecular network of ChAc:U is beyond the scope of the present paper and will be deepened in a separate work on hydrated ChAc:U. Here the focus is on the role of the DES constituents - choline, acetate and urea - and we can safely assume that the residual water molecules will participate in the intermolecular network without drastic alterations of the mutual relationships among them.

In order to monitor the translational mobility and gather a more complete overview of the system, the self-diffusion coefficients of the different ChAc:U moieties were measured by PFG NMR. The diffusivities, D, probed in the range 278 – 358 K are given in **Figure S6** and **Table S2** in the Supporting Information. As expected, the diffusion coefficients measured for the methylene protons of choline yielded the same value as CH_3, hence only the latter is presented. The temperature dependence of the diffusion coefficients over the whole probed temperature range was modelled in terms of an Arrhenius-activated process. Translational activation energies are reported in **Figure 10** and fit parameters in **Table S3** in the Supporting Information. While the activation energies associated with relaxation data are in the range 10−30 kJ mol^{-1}, the activation energies associated with diffusion data are larger (40−50 kJ mol^{-1}). This is due to the different molecular motion affecting these apparent activation energies, rotational *versus* translational, and is in agreement with behaviours found for instance in ionic liquids. [66,67] Noteworthy is the order of E_a^{transl}: urea ≈ H_2O + OH > acetate > choline. This is unrelated to the molecular size of the species and can be explained only by admitting that the translational motion of urea and acetate is slowed down by their strong involvement in the HB network. The major role of urea and acetate in the intermolecular network, inferred here from a dynamic parameter, fits the molecular picture outlined by means of more common techniques for structure elucidation, such as X-ray and NOESY. Note, also, that this prominent role is maintained here even in the presence of residual amounts of water (5.7 wt%). Contrarily, the activation energy of choline is the lowest one

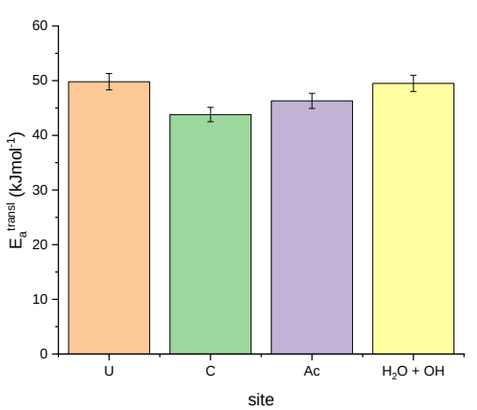

Figure 10. Translational activation energy E_a^{transl} (kJmol^{-1}) obtained for all species in ChAc:U.

regardless of its higher size due to its less fundamental role in the intermolecular connections. As urea has proven to strongly connect with other constituents in several DES using both the oxygen and proton nuclei (see also the linear Sankey diagram in **Figure 6**), its reduced rotational and translational mobility (high E_a^{rot} and E_a^{transl}) is quite expected. The peculiar role of acetate is instead not a foregone conclusion. The key role of this small anion in the HB network keeps it on a tight leash, strongly affecting its translational mobility and increasing its E_a^{transl}, which is a dynamic indicator of the whole molecule. Contrarily, the rotational mobility of the methyl protons of acetate does not suffer from a strong effect, as they are not directly participating in the HB network. Hence the corresponding E_a^{rot} - a local dynamic parameter - is still smaller than the rotational activation energy of all other proton sites of both choline and urea.

Conclusion.

Choline acetate mixtures with urea at a stoichiometric composition of 1:2 are deep eutectic media, whose melting point is ca. 40 °C, but it can be easily supercooled into the liquid state at sub-ambient conditions. Liquid ChAc:U structure at atomistic level has been investigated by means of synchrotron high energy X-ray diffraction, supported by the EPSR Reverse Monte Carlo analysis approach that allows extracting detailed information on the mutual interactions between ChAc:U's moieties. Hydrogen bonding plays a major role in determining structure in liquid ChAc:U. Radial distribution functions shows how acetate-mediated HB are among the strongest in the system; urea plays also a major role as HB donor and these correlations are straightforwardly described by the use of a Sankey diagram illustrating HB flow among the different donor and acceptor moieties. A complex intertwining of different moieties is observed with coulombic interactions (via HB correlations) mostly involving acetate and urea, while choline is involved mostly in dispersive interactions. This peculiar situation is mirrored in the dynamics monitored in ChAc:U. While acetate's methyl group shows the lowest correlation times and activation energy considering ^{1}H rotational motion, the anion diffuses slower than expected from its size, thus confirming its strong role in the HB network. Choline turns out to be the moiety with the lowest activation energy concerning diffusive dynamics, reflecting its secondary involvement into the HB interactions network.

Supplementary Material.

Combined distribution functions accounting for the hydrogen bonding geometries; NMR plots and tables; EPSR force field parameters.

Acknowledgements.

This work has been supported by the University of Rome Sapienza Projects: "Microscopic and mesoscopic organization in ionic liquid-based systems." (RG11715C7CC660BE) and "Green solvents for simple and complex carbohydrates" (RM120172B2165468).

M.B. acknowledges financial support by the Deutsche Forschungsgemeinschaft (DFG) through project Br 5494/1-1.

M.E.D.P. thanks Politecnico di Milano for her postdoctoral fellowship in the framework of the "MSCA EF Master Class 2018" funding programme.

Access to Prof. S. Brutti's laboratories (Univ. Rome – Sapienza) is gratefully acknowledged.

We thank Diamond Light Source for access to beamline I15-1 (CY27222-1) that contributed to the results presented here.

DATA AVAILABILITY.

The data that support the findings of this study are available from the corresponding authors upon reasonable request.

References

(1) Abbott, A. P.; Capper, G.; Davies, D. L.; Rasheed, R. K.; Tambyrajah, V. Novel Solvent Properties of Choline Chloride/Urea Mixtures. *Chem. Commun.* **2003**, No. 1, 70–71. https://doi.org/10.1039/b210714g.

(2) Abbott, A. P.; Boothby, D.; Capper, G.; Davies, D. L.; Rasheed, R. K. Deep Eutectic Solvents Formed between Choline Chloride and Carboxylic Acids: Versatile Alternatives to Ionic Liquids. *J. Am. Chem. Soc.* **2004**, *126* (29), 9142–9147. https://doi.org/10.1021/ja048266j.

(3) Smith, E. L.; Abbott, A. P.; Ryder, K. S. Deep Eutectic Solvents (DESs) and Their Applications. *Chem. Rev.* **2014**, *114* (21), 11060–11082. https://doi.org/10.1021/cr300162p.

(4) Wagle, D. V.; Zhao, H.; Baker, G. A. Deep Eutectic Solvents: Sustainable Media for Nanoscale and Functional Materials. *Acc. Chem. Res.* **2014**, *47* (8), 2299–2308. https://doi.org/10.1021/ar5000488.

(5) Zhang, Q.; De Oliveira Vigier, K.; Royer, S.; Jérôme, F. Deep Eutectic Solvents: Syntheses, Properties and Applications. *Chem. Soc. Rev.* **2012**, *41* (21), 7108–7146. https://doi.org/10.1039/c2cs35178a.

(6) Paiva, A.; Craveiro, R.; Aroso, I.; Martins, M.; Reis, R. L.; Duarte, A. R. C. Natural Deep Eutectic Solvents - Solvents for the 21st Century. *ACS Sustain. Chem. Eng.* **2014**, *2* (5), 1063–1071. https://doi.org/10.1021/sc500096j.

(7) Roda, A.; Matias, A.; Paiva, A.; Duarte, A. Polymer Science and Engineering Using Deep Eutectic Solvents. *Polymers (Basel).* **2019**, *11* (5), 912. https://doi.org/10.3390/polym11050912.

(8) Perna, F. M.; Vitale, P.; Capriati, V. Deep Eutectic Solvents and Their Applications as Green Solvents. *Curr. Opin. Green Sustain. Chem.* **2020**, *21*, 27–33. https://doi.org/10.1016/j.cogsc.2019.09.004.

(9) Perkins, S. L.; Painter, P.; Colina, C. M. Molecular Dynamic Simulations and Vibrational Analysis of an Ionic Liquid Analogue. *J. Phys. Chem. B* **2013**, *117* (35), 10250–10260. https://doi.org/10.1021/jp404619x.

(10) Hammond, O. S.; Bowron, D. T.; Edler, K. J. Liquid Structure of the Choline Chloride-Urea

Deep Eutectic Solvent (Reline) from Neutron Diffraction and Atomistic Modelling. *Green Chem.* **2016**, *18* (9), 2736–2744. https://doi.org/10.1039/c5gc02914g.

(11) Gilmore, M.; Moura, L. M.; Turner, A. H.; Swadźba-Kwaśny, M.; Callear, S. K.; McCune, J. A.; Scherman, O. A.; Holbrey, J. D. A Comparison of Choline:Urea and Choline:Oxalic Acid Deep Eutectic Solvents at 338 K. *J. Chem. Phys.* **2018**, *148* (19). https://doi.org/10.1063/1.5010246.

(12) Fetisov, E. O.; Harwood, D. B.; Kuo, I. F. W.; Warrag, S. E. E.; Kroon, M. C.; Peters, C. J.; Siepmann, J. I. First-Principles Molecular Dynamics Study of a Deep Eutectic Solvent: Choline Chloride/Urea and Its Mixture with Water. *J. Phys. Chem. B* **2018**, *122* (3), 1245–1254. https://doi.org/10.1021/acs.jpcb.7b10422.

(13) Kaur, S.; Sharma, S.; Kashyap, H. K.; Kaur, S.; Sharma, S.; Kashyap, H. K. Bulk and Interfacial Structures of Reline Deep Eutectic Solvent : A Molecular Dynamics Study Bulk and Interfacial Structures of Reline Deep Eutectic Solvent : A Molecular Dynamics Study. *J. Chem. Phys.* **2017**, *147*, 194507. https://doi.org/10.1063/1.4996644.

(14) Ashworth, C. R.; Matthews, R. P.; Welton, T.; Hunt, P. A. Doubly Ionic Hydrogen Bond Interactions within the Choline Chloride-Urea Deep Eutectic Solvent. *Phys. Chem. Chem. Phys.* **2016**, *18* (27), 18145–18160. https://doi.org/10.1039/c6cp02815b.

(15) Triolo, A.; Lo Celso, F.; Russina, O. Structural Features of β-Cyclodextrin Solvation in the Deep Eutectic Solvent, Reline. *J. Phys. Chem. B* **2020**, *124* (13), 2652–2660. https://doi.org/10.1021/acs.jpcb.0c00876.

(16) Di Pietro, M. E.; Hammond, O.; van den Bruinhorst, A.; Mannu, A.; Padua, A.; Mele, A.; Costa Gomes, M. Connecting Chloride Solvation with Hydration in Deep Eutectic Systems. *Phys. Chem. Chem. Phys.* **2021**, *23* (1), 107–111. https://doi.org/10.1039/D0CP05843B.

(17) Gilmore, M.; Swadzba-Kwasny, M.; Holbrey, J. D. Thermal Properties of Choline Chloride/Urea System Studied under Moisture-Free Atmosphere. *J. Chem. Eng. Data* **2019**, *64* (12), 5248–5255. https://doi.org/10.1021/acs.jced.9b00474.

(18) Gabriele, F.; Chiarini, M.; Germani, R.; Tiecco, M.; Spreti, N. Effect of Water Addition on Choline Chloride/Glycol Deep Eutectic Solvents: Characterization of Their Structural and Physicochemical Properties. *J. Mol. Liq.* **2019**, *291*, 111301.

https://doi.org/10.1016/j.molliq.2019.111301.

(19) Wagle, D. V.; Baker, G. A.; Mamontov, E. Differential Microscopic Mobility of Components within a Deep Eutectic Solvent. *J. Phys. Chem. Lett.* **2015**, *6* (15), 2924–2928. https://doi.org/10.1021/acs.jpclett.5b01192.

(20) Stefanovic, R.; Ludwig, M.; Webber, G. B.; Atkin, R.; Page, A. J. Nanostructure, Hydrogen Bonding and Rheology in Choline Chloride Deep Eutectic Solvents as a Function of the Hydrogen Bond Donor. *Phys. Chem. Chem. Phys.* **2017**, *19* (4), 3297–3306. https://doi.org/10.1039/c6cp07932f.

(21) Turner, A. H.; Holbrey, J. D. Investigation of Glycerol Hydrogen-Bonding Networks in Choline Chloride/Glycerol Eutectic-Forming Liquids Using Neutron Diffraction. *Phys. Chem. Chem. Phys.* **2019**, *21* (39), 21782–21789. https://doi.org/10.1039/c9cp04343h.

(22) Perkins, S. L.; Painter, P.; Colina, C. M. Experimental and Computational Studies of Choline Chloride-Based Deep Eutectic Solvents. *J. Chem. Eng. Data* **2014**, *59* (11), 3652–3662. https://doi.org/10.1021/je500520h.

(23) Kaur, S.; Malik, A.; Kashyap, H. K. Anatomy of Microscopic Structure of Ethaline Deep Eutectic Solvent Decoded through Molecular Dynamics Simulations. *J. Phys. Chem. B* **2019**, *123* (39), 8291–8299. https://doi.org/10.1021/acs.jpcb.9b06624.

(24) Zhang, Y.; Poe, D.; Heroux, L.; Squire, H.; Doherty, B. W.; Long, Z.; Dadmun, M.; Gurkan, B.; Tuckerman, M. E.; Maginn, E. J. Liquid Structure and Transport Properties of the Deep Eutectic Solvent Ethaline. *J. Phys. Chem. B* **2020**, *124* (25), 5251–5264. https://doi.org/10.1021/acs.jpcb.0c04058.

(25) Zhang, H.; Ferrer, M. L.; Roldán-Ruiz, M. J.; Jiménez-Riobóo, R. J.; Gutiérrez, M. C.; Del Monte, F. SI - Brillouin Spectroscopy as a Suitable Technique for the Determination of the Eutectic Composition in Mixtures of Choline Chloride and Water. *J. Phys. Chem. B* **2020**, *124* (19), 4002–4009. https://doi.org/10.1021/acs.jpcb.0c01919.

(26) Rahman, M. S.; Raynie, D. E. Thermal Behavior, Solvatochromic Parameters, and Metal Halide Solvation of the Novel Water-Based Deep Eutectic Solvents. *J. Mol. Liq.* **2020**, *3*, 114779. https://doi.org/10.1016/j.molliq.2020.114779.

(27) Triolo, A.; Lo Celso, F.; Brehm, M.; Di Lisio, V.; Russina, O. Liquid Structure of a Choline Chloride-Water Natural Deep Eutectic Solvent: A Molecular Dynamics Characterization. *J. Mol. Liq.* **2021**, *331*, 115750. https://doi.org/10.1016/j.molliq.2021.115750.

(28) Fukaya, Y.; Iizuka, Y.; Sekikawa, K.; Ohno, H. Bio Ionic Liquids: Room Temperature Ionic Liquids Composed Wholly of Biomaterials. *Green Chem.* **2007**, *9* (11), 1155–1157. https://doi.org/10.1039/b706571j.

(29) Zhao, H.; Baker, G. A.; Holmes, S. New Eutectic Ionic Liquids for Lipase Activation and Enzymatic Preparation of Biodiesel. *Org. Biomol. Chem.* **2011**, *9* (6), 1908–1916. https://doi.org/10.1039/c0ob01011a.

(30) Hoppe, J.; Drozd, R.; Byzia, E.; Smiglak, M. Deep Eutectic Solvents Based on Choline Cation - Physicochemical Properties and Influence on Enzymatic Reaction with β-Galactosidase. *Int. J. Biol. Macromol.* **2019**, *136*, 296–304. https://doi.org/10.1016/j.ijbiomac.2019.06.027.

(31) Colombo Dugoni, G.; Mezzetta, A.; Guazzelli, L.; Chiappe, C.; Ferro, M.; Mele, A. Purification of Kraft Cellulose under Mild Conditions Using Choline Acetate Based Deep Eutectic Solvents. *Green Chem.* **2020**, 8680–8691. https://doi.org/10.1039/d0gc03375h.

(32) Filik, J.; Ashton, A. W.; Chang, P. C. Y.; Chater, P. A.; Day, S. J.; Drakopoulos, M.; Gerring, M. W.; Hart, M. L.; Magdysyuk, O. V.; Michalik, S.; Smith, A.; Tang, C. C.; Terrill, N. J.; Wharmby, M. T.; Wilhelm, H. Processing Two-Dimensional X-Ray Diffraction and Small-Angle Scattering Data in DAWN 2. *J. Appl. Crystallogr.* **2017**, *50* (3), 959–966. https://doi.org/10.1107/S1600576717004708.

(33) Soper, A. K.; Barney, E. R. Extracting the Pair Distribution Function from White-Beam X-Ray Total Scattering Data. *J. Appl. Crystallogr.* **2011**, *44* (4), 714–726. https://doi.org/10.1107/S0021889811021455.

(34) Soper, A. K. The Radial Distribution Functions of Water as Derived from Radiation Total Scattering Experiments: Is There Anything We Can Say for Sure? *ISRN Phys. Chem.* **2013**, *2013*, 1–67. https://doi.org/10.1155/2013/279463.

(35) Soper, A. K. Empirical Potential Monte Carlo Simulation of Fluid Structure. *Chem. Phys.* **1996**, *202* (2–3), 295–306. https://doi.org/10.1016/0301-0104(95)00357-6.

588 (36) Soper, A. K.; Castner, E. W.; Luzar, A. Impact of Urea on Water Structure: A Clue to Its
589 Properties as a Denaturant? *Biophys. Chem.* **2003**, *105* (2–3), 649–666.
590 https://doi.org/10.1016/S0301-4622(03)00095-4.

591 (37) Bowron, D. T.; D'Agostino, C.; Gladden, L. F.; Hardacre, C.; Holbrey, J. D.; Lagunas, M. C.;
592 McGregor, J.; Mantle, M. D.; Mullan, C. L.; Youngs, T. G. A. Structure and Dynamics of 1-
593 Ethyl-3-Methylimidazolium Acetate via Molecular Dynamics and Neutron Diffraction. *J. Phys.*
594 *Chem. B* **2010**, *114* (23), 7760–7768. https://doi.org/10.1021/jp102180q.

595 (38) Brehm, M.; Kirchner, B. TRAVIS - A Free Analyzer and Visualizer for Monte Carlo and
596 Molecular Dynamics Trajectories. *J. Chem. Inf. Model.* **2011**, *51* (8), 2007–2023.
597 https://doi.org/10.1021/ci200217w.

598 (39) Brehm, M.; Thomas, M.; Gehrke, S.; Kirchner, B. TRAVIS—A Free Analyzer for Trajectories
599 from Molecular Simulation. *J. Chem. Phys.* **2020**, *152* (16), 164105.
600 https://doi.org/10.1063/5.0005078.

601 (40) Hollõczki, O.; Macchiagodena, M.; Weber, H.; Thomas, M.; Brehm, M.; Stark, A.; Russina, O.;
602 Triolo, A.; Kirchner, B. Triphilic Ionic-Liquid Mixtures: Fluorinated and Non-Fluorinated
603 Aprotic Ionic-Liquid Mixtures. *ChemPhysChem* **2015**, *16* (15), 3325–3333.
604 https://doi.org/10.1002/cphc.201500473.

605 (41) Kaur, S.; Sharma, S.; Kashyap, H. K. Bulk and Interfacial Structures of Reline Deep Eutectic
606 Solvent: A Molecular Dynamics Study. *J. Chem. Phys.* **2017**, *147* (19).
607 https://doi.org/10.1063/1.4996644.

608 (42) Kumari, P.; Shobhna; Kaur, S.; Kashyap, H. K. Influence of Hydration on the Structure of
609 Reline Deep Eutectic Solvent: A Molecular Dynamics Study. *ACS Omega* **2018**, *3* (11), 15246–
610 15255. https://doi.org/10.1021/acsomega.8b02447.

611 (43) Hammond, O. S.; Bowron, D. T.; Edler, K. J. The Effect of Water upon Deep Eutectic Solvent
612 Nanostructure: An Unusual Transition from Ionic Mixture to Aqueous Solution. *Angew. Chemie*
613 *- Int. Ed.* **2017**, *56* (33), 9782–9785. https://doi.org/10.1002/anie.201702486.

614 (44) McDonald, S.; Murphy, T.; Imberti, S.; Warr, G. G.; Atkin, R. Amphiphilically Nanostructured
615 Deep Eutectic Solvents. *J. Phys. Chem. Lett.* **2018**, *9* (14), 3922–3927.

https://doi.org/10.1021/acs.jpclett.8b01720.

(45) Triolo, A.; Russina, O.; Bleif, H. J.; Di Cola, E. Nanoscale Segregation in Room Temperature Ionic Liquids. *J. Phys. Chem. B* **2007**, *111* (18), 4641–4644. https://doi.org/10.1021/jp067705t.

(46) Russina, O.; Triolo, A.; Gontrani, L.; Caminiti, R. Mesoscopic Structural Heterogeneities in Room-Temperature Ionic Liquids. *J. Phys. Chem. Lett.* **2012**, *3* (1), 27–33. https://doi.org/10.1021/jz201349z.

(47) Macchiagodena, M.; Ramondo, F.; Triolo, A.; Gontrani, L.; Caminiti, R. Liquid Structure of 1-Ethyl-3-Methylimidazolium Alkyl Sulfates by x-Ray Scattering and Molecular Dynamics. *J. Phys. Chem. B* **2012**, *116* (45), 13448–13458. https://doi.org/10.1021/jp306982e.

(48) Russina, O.; Sferrazza, A.; Caminiti, R.; Triolo, A. Amphiphile Meets Amphiphile: Beyond the Polar-Apolar Dualism in Ionic Liquid/Alcohol Mixtures. *J. Phys. Chem. Lett.* **2014**, *5* (10), 1738–1742. https://doi.org/10.1021/jz500743v.

(49) Schroer, W.; Triolo, A.; Russina, O. Nature of Mesoscopic Organization in Protic Ionic Liquid-Alcohol Mixtures. *J. Phys. Chem. B* **2016**, *120* (9), 2638–2643. https://doi.org/10.1021/acs.jpcb.6b01422.

(50) Russina, O.; Lo Celso, F.; Plechkova, N. V.; Triolo, A. Emerging Evidences of Mesoscopic-Scale Complexity in Neat Ionic Liquids and Their Mixtures. *J. Phys. Chem. Lett.* **2017**, *8* (6), 1197–1204. https://doi.org/10.1021/acs.jpclett.6b02811.

(51) Hammond, O. S.; Bowron, D. T.; Jackson, A. J.; Arnold, T.; Sanchez-Fernandez, A.; Tsapatsaris, N.; Garcia Sakai, V.; Edler, K. J. Resilience of Malic Acid Natural Deep Eutectic Solvent Nanostructure to Solidification and Hydration. *J. Phys. Chem. B* **2017**, *121* (31), 7473–7483. https://doi.org/10.1021/acs.jpcb.7b05454.

(52) Posada, E.; Roldán-Ruiz, M. J.; Jiménez Riobóo, R. J.; Gutiérrez, M. C.; Ferrer, M. L.; del Monte, F. Nanophase Separation in Aqueous Dilutions of a Ternary DES as Revealed by Brillouin and NMR Spectroscopy. *J. Mol. Liq.* **2019**, *276*, 196–203. https://doi.org/10.1016/j.molliq.2018.11.139.

(53) Hall, C. A.; Le, K. A.; Rudaz, C.; Radhi, A.; Lovell, C. S.; Damion, R. A.; Budtova, T.; Ries, M. E. Macroscopic and Microscopic Study of 1-Ethyl-3-Methyl-Imidazolium Acetate-Water

644 Mixtures. *J. Phys. Chem. B* **2012**, *116* (42), 12810–12818. https://doi.org/10.1021/jp306829c.

645 (54) Grzesiek, S.; Becker, E. D. Hydrogen Bonding. In *Encyclopedia of Magnetic Resonance*; John
646 Wiley & Sons, Ltd: Chichester, UK, 2011.
647 https://doi.org/10.1002/9780470034590.emrstm0216.pub2.

648 (55) Häkkinen, R.; Alshammari, O.; Timmermann, V.; D'Agostino, C.; Abbott, A. Nanoscale
649 Clustering of Alcoholic Solutes in Deep Eutectic Solvents Studied by Nuclear Magnetic
650 Resonance and Dynamic Light Scattering. *ACS Sustain. Chem. Eng.* **2019**, *7* (17), 15086–15092.
651 https://doi.org/10.1021/acssuschemeng.9b03771.

652 (56) Delso, I.; Lafuente, C.; Muñoz-Embid, J.; Artal, M. NMR Study of Choline Chloride-Based
653 Deep Eutectic Solvents. *J. Mol. Liq.* **2019**, *290*. https://doi.org/10.1016/j.molliq.2019.111236.

654 (57) Bloembergen, N.; Purcell, E. M.; Pound, R. V. Relaxation Effects in Nuclear Magnetic
655 Resonance Absorption. *Phys. Rev.* **1948**, *73* (7), 679–712.
656 https://doi.org/10.1103/PhysRev.73.679.

657 (58) Hayamizu, K.; Tsuzuki, S.; Seki, S.; Umebayashi, Y. Nuclear Magnetic Resonance Studies on
658 the Rotational and Translational Motions of Ionic Liquids Composed of 1-Ethyl-3-
659 Methylimidazolium Cation and Bis(Trifluoromethanesulfonyl)Amide and
660 Bis(Fluorosulfonyl)Amide Anions and Their Binary Systems Including Li. *J. Chem. Phys.* **2011**,
661 *135* (8). https://doi.org/10.1063/1.3625923.

662 (59) Hayamizu, K.; Tsuzuki, S.; Seki, S.; Umebayashi, Y. Multinuclear NMR Studies on
663 Translational and Rotational Motion for Two Ionic Liquids Composed of BF4 Anion. *J. Phys.*
664 *Chem. B* **2012**, *116* (36), 11284–11291. https://doi.org/10.1021/jp306146s.

665 (60) Alam, T. M.; Dreyer, D. R.; Bielwaski, C. W.; Ruoff, R. S. Measuring Molecular Dynamics and
666 Activation Energies for Quaternary Acyclic Ammonium and Cyclic Pyrrolidinium Ionic Liquids
667 Using 14N NMR Spectroscopy. *J. Phys. Chem. A* **2011**, *115* (17), 4307–4316.
668 https://doi.org/10.1021/jp200630k.

669 (61) Di Pietro, M. E.; Castiglione, F.; Mele, A. Polar/Apolar Domains' Dynamics in
670 Alkylimidazolium Ionic Liquids Unveiled by the Dual Receiver NMR 1H and 19F Relaxation
671 Experiment. *J. Mol. Liq.* **2021**, *322*, 114567. https://doi.org/10.1016/j.molliq.2020.114567.

(62) Bystrov, S. S.; Matveev, V. V.; Chernyshev, Y. S.; Balevičius, V.; Chizhik, V. I. Molecular Mobility in a Set of Imidazolium-Based Ionic Liquids [Bmim]+A- by the NMR-Relaxation Method. *J. Phys. Chem. B* **2019**, *123* (10), 2362–2372. https://doi.org/10.1021/acs.jpcb.8b11250.

(63) Shimizu, Y.; Wachi, Y.; Fujii, K.; Imanari, M.; Nishikawa, K. NMR Study on Ion Dynamics and Phase Behavior of a Piperidinium-Based Room-Temperature Ionic Liquid: 1-Butyl-1-Methylpiperidinium Bis(Fluorosulfonyl)Amide. *J. Phys. Chem. B* **2016**, *120* (25), 5710–5719. https://doi.org/10.1021/acs.jpcb.6b04095.

(64) Antony, J. H.; Mertens, D.; Dölle, A.; Wasserscheid, P.; Carper, W. R. Molecular Reorientational Dynamics of the Neat Ionic Liquid 1-Butyl-3-Methylimidazolium Hexafluorophosphate by Measurement of 13C Nuclear Magnetic Relaxation Data. *ChemPhysChem* **2003**, *4* (6), 588–594. https://doi.org/10.1002/cphc.200200603.

(65) Bayley, P. M.; Best, A. S.; MacFarlane, D. R.; Forsyth, M. The Effect of Coordinating and Non-Coordinating Additives on the Transport Properties in Ionic Liquid Electrolytes for Lithium Batteries. *Phys. Chem. Chem. Phys.* **2011**, *13* (10), 4632–4640. https://doi.org/10.1039/c0cp02084b.

(66) Hayamizu, K.; Tsuzuki, S.; Seki, S.; Fujii, K.; Suenaga, M.; Umebayashi, Y. Studies on the Translational and Rotational Motions of Ionic Liquids Composed of N-Methyl-N-Propyl-Pyrrolidinium (P13) Cation and Bis(Trifluoromethanesulfonyl)Amide and Bis(Fluorosulfonyl)Amide Anions and Their Binary Systems Including Lithium Salts. *J. Chem. Phys.* **2010**, *133* (19), 194505. https://doi.org/10.1063/1.3505307.

(67) Di Pietro, M. E.; Castiglione, F.; Mele, A. Anions as Dynamic Probes for Ionic Liquid Mixtures. *J. Phys. Chem. B* **2020**, *124* (14), 2879–2891. https://doi.org/10.1021/acs.jpcb.0c00026.

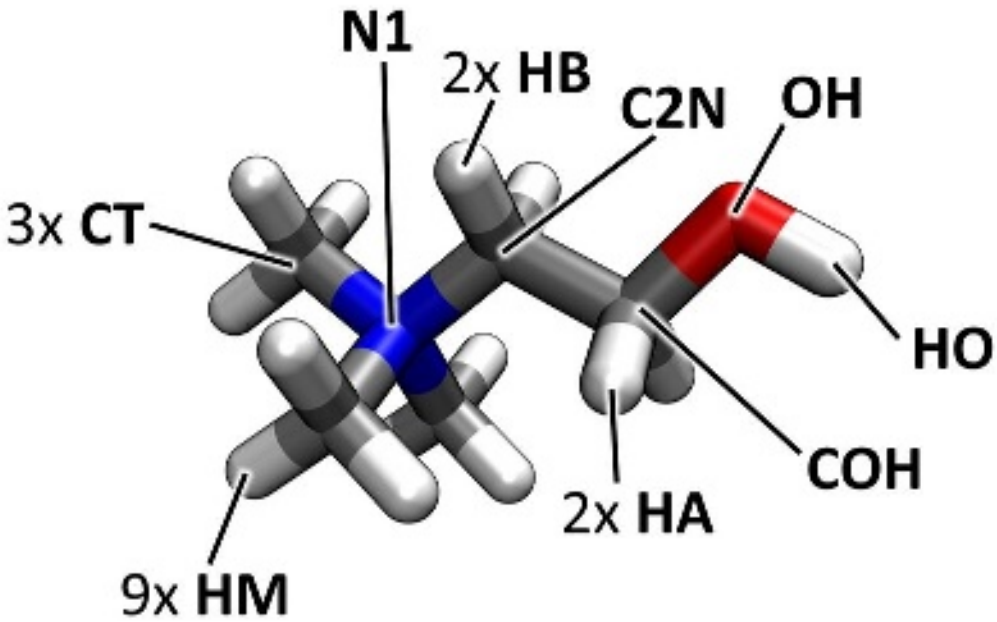
N1
2x HB
C2N
OH
3x CT
HO
COH
2x HA
9x HM

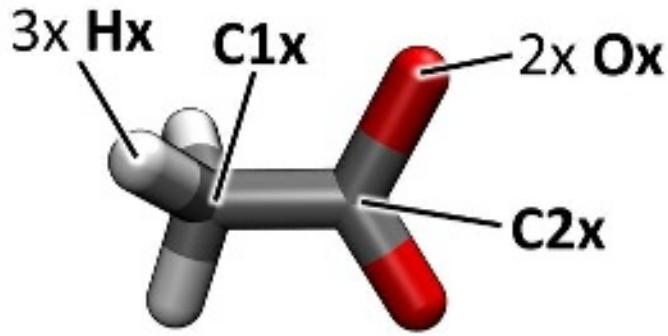
3x Hx
C1x
2x Ox
C2x

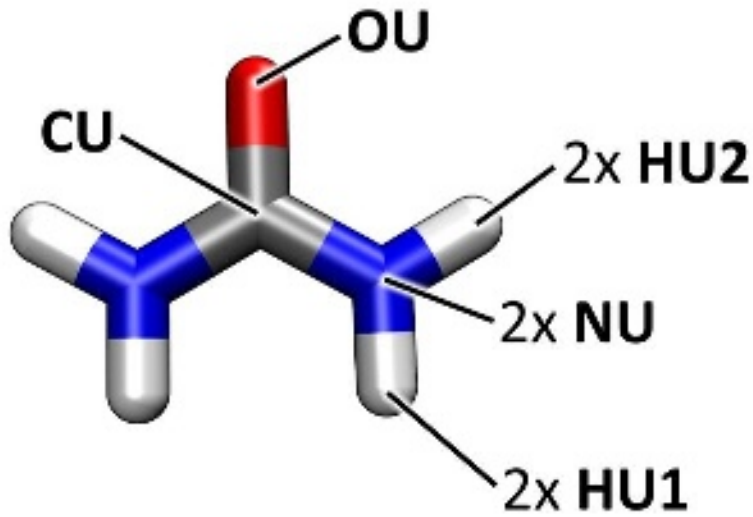
OU
CU
2x HU2
2x NU
2x HU1

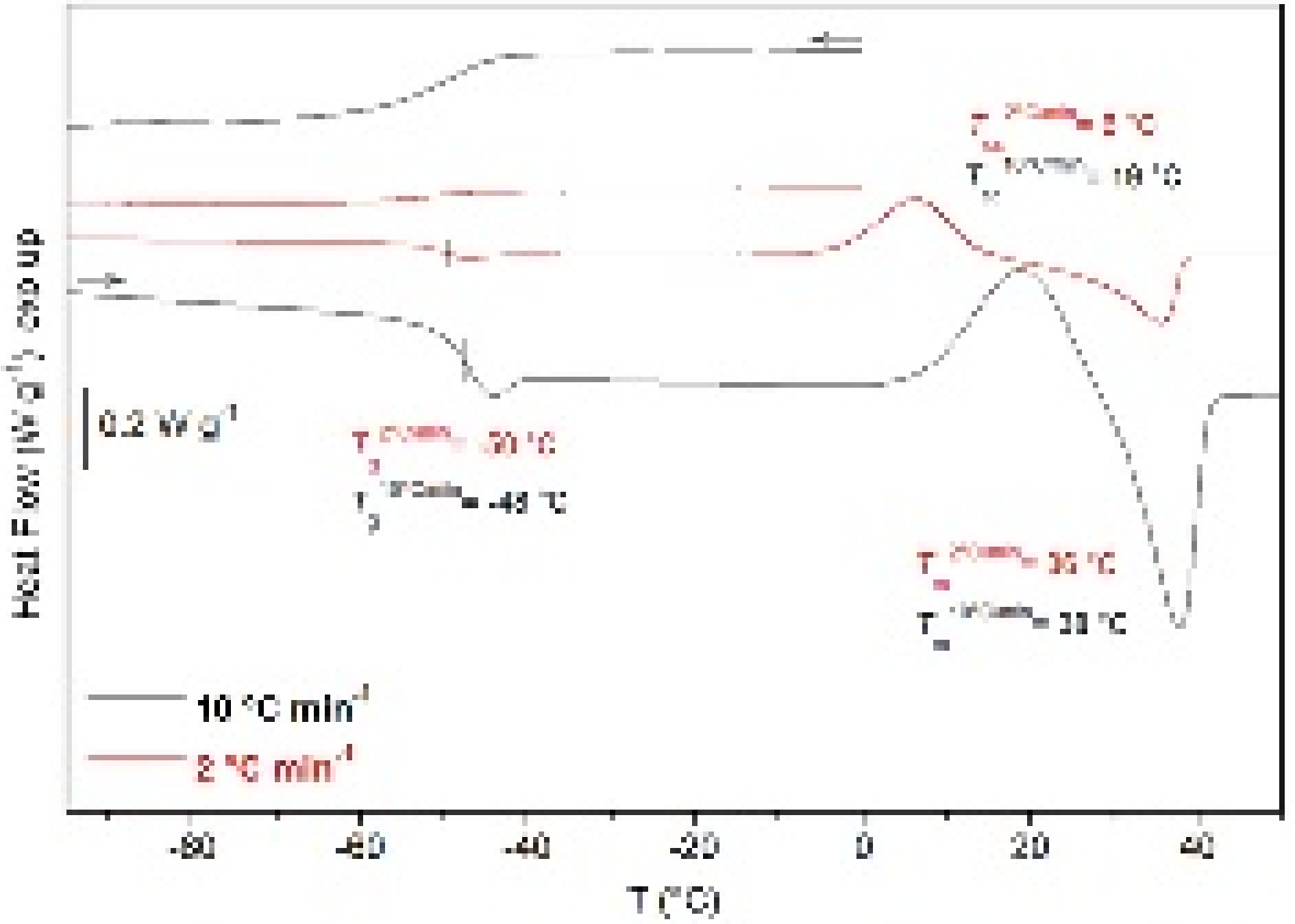
0.2 W g⁻¹
10 °C min⁻¹
2 °C min⁻¹
-60
-40
-20
0
20
40
T (°C)

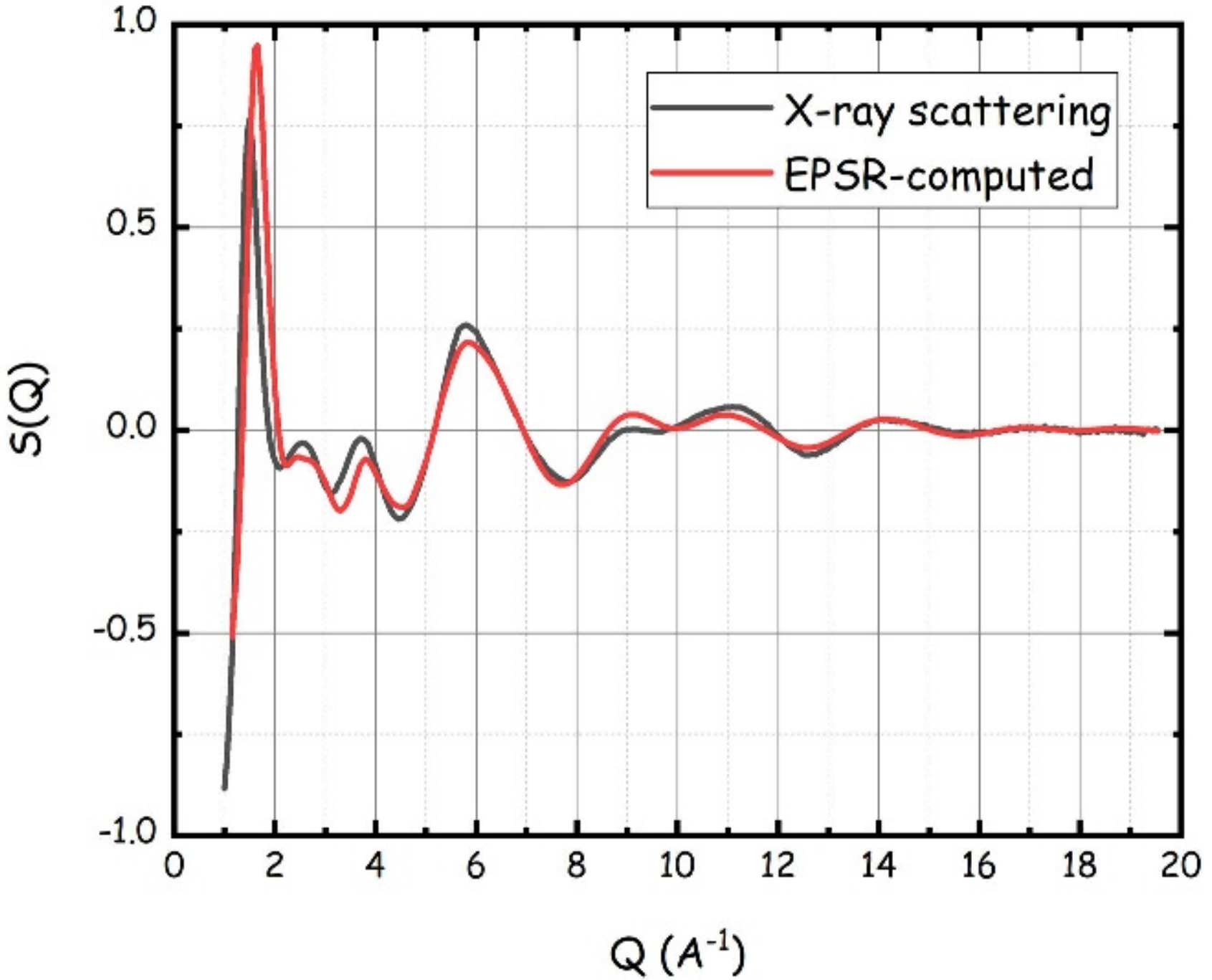
1.0
0.5
0.0
-0.5
-1.0
S(Q)
0
2
4
6
8
10
12
14
16
18
20
Q (A-1)
X-ray scattering
EPSR-computed

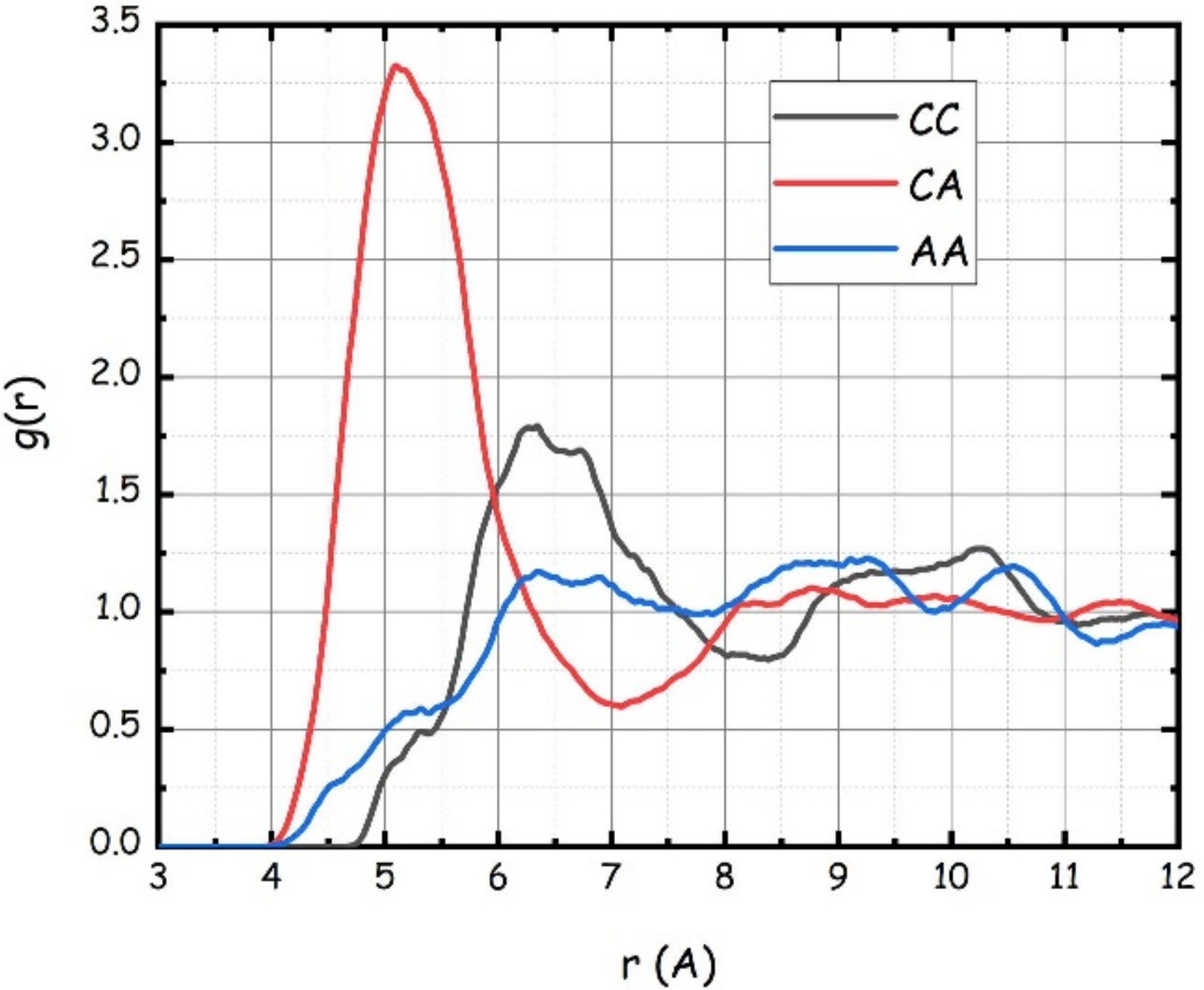
3.5
3.0
2.5
2.0
1.5
1.0
0.5
0.0
g(r)
3
4
5
6
7
8
9
10
11
12
r (A)
CC
CA
AA

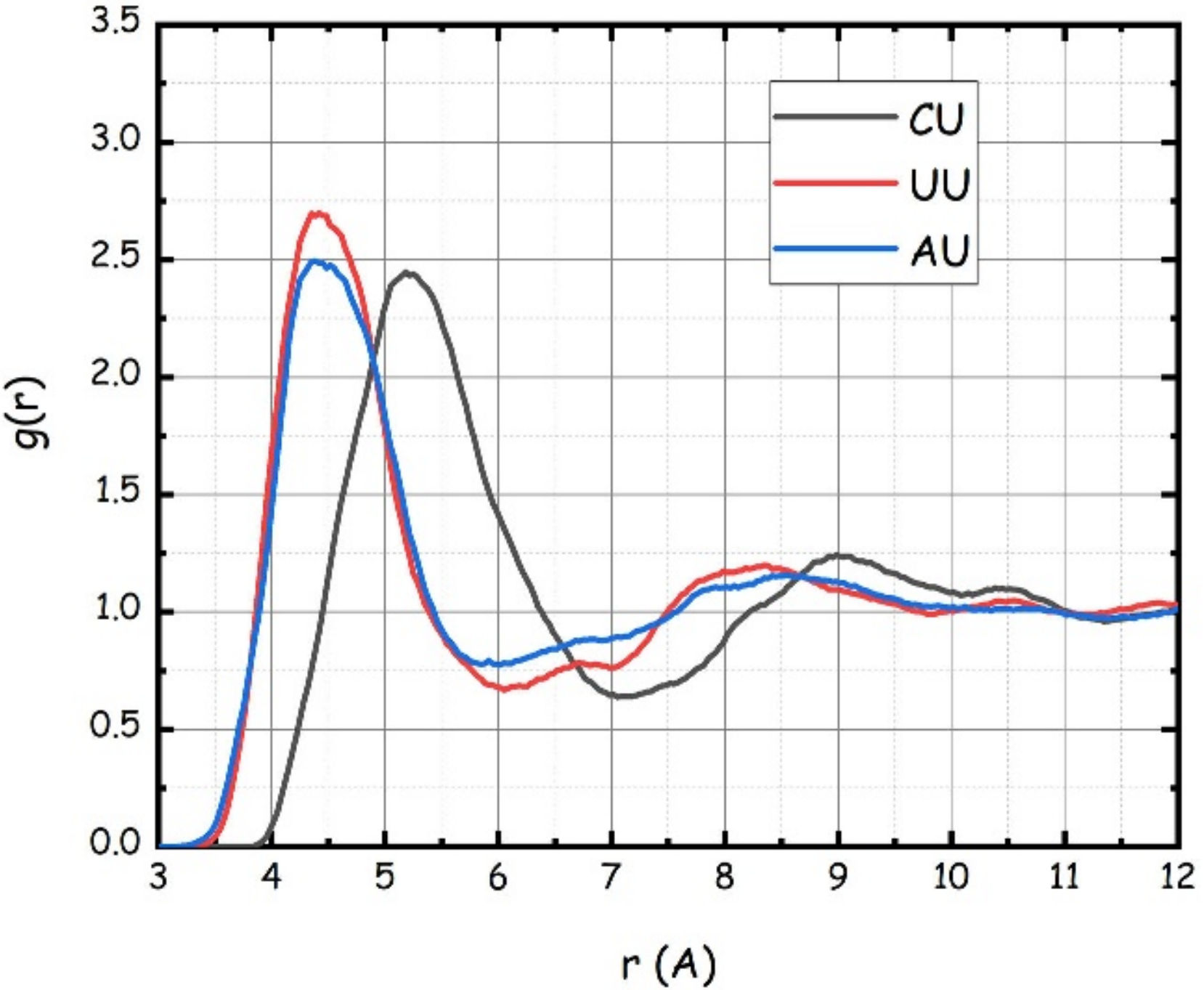
3.5
3.0
2.5
2.0
1.5
1.0
0.5
0.0
g(r)
3
4
5
6
7
8
9
10
11
12
r (A)
CU
UU
AU

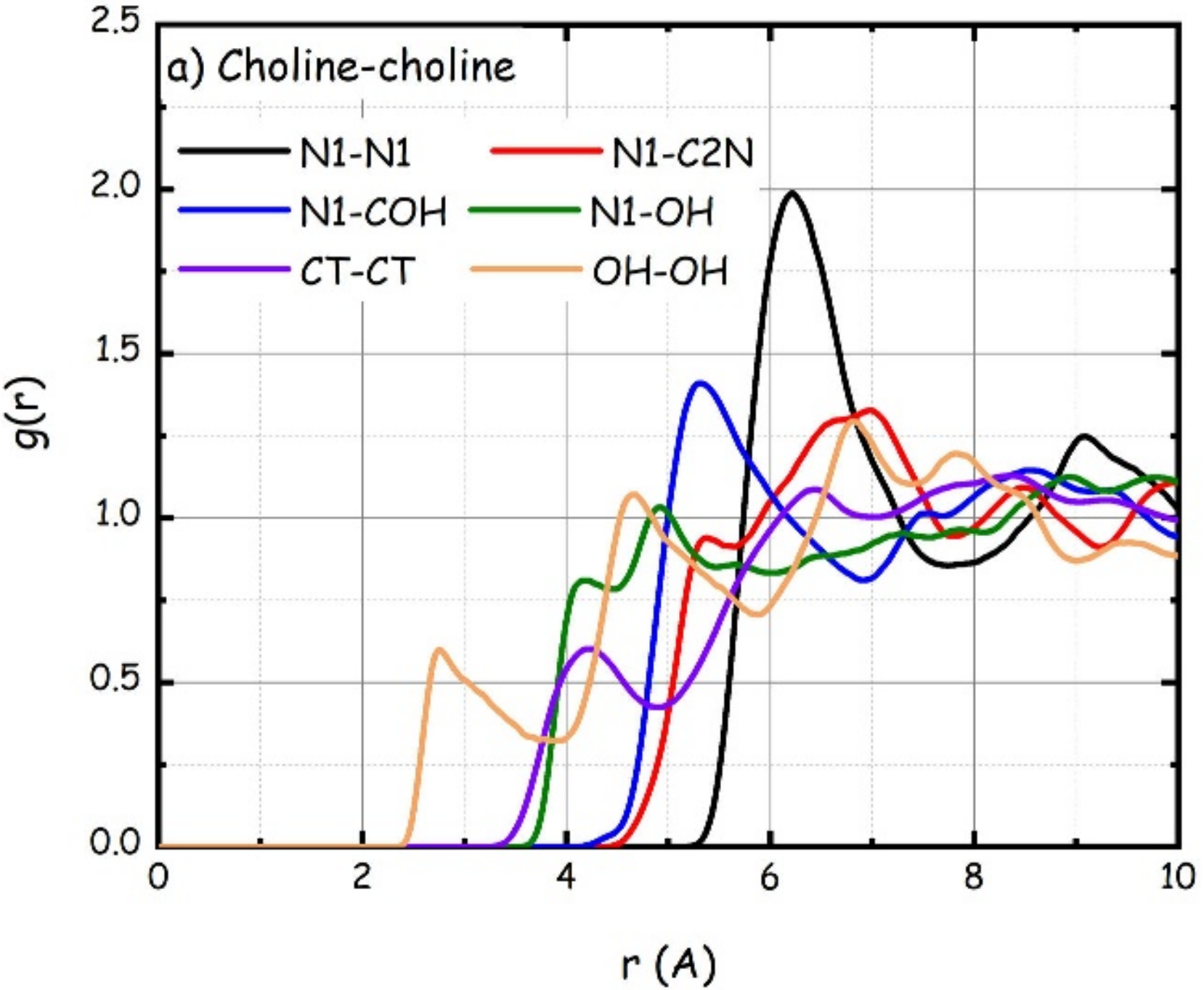
a) Choline-choline
N1-N1
N1-C2N
N1-COH
N1-OH
CT-CT
OH-OH
g(r)
r (A)
0.0
0.5
1.0
1.5
2.0
2.5
0
2
4
6
8
10

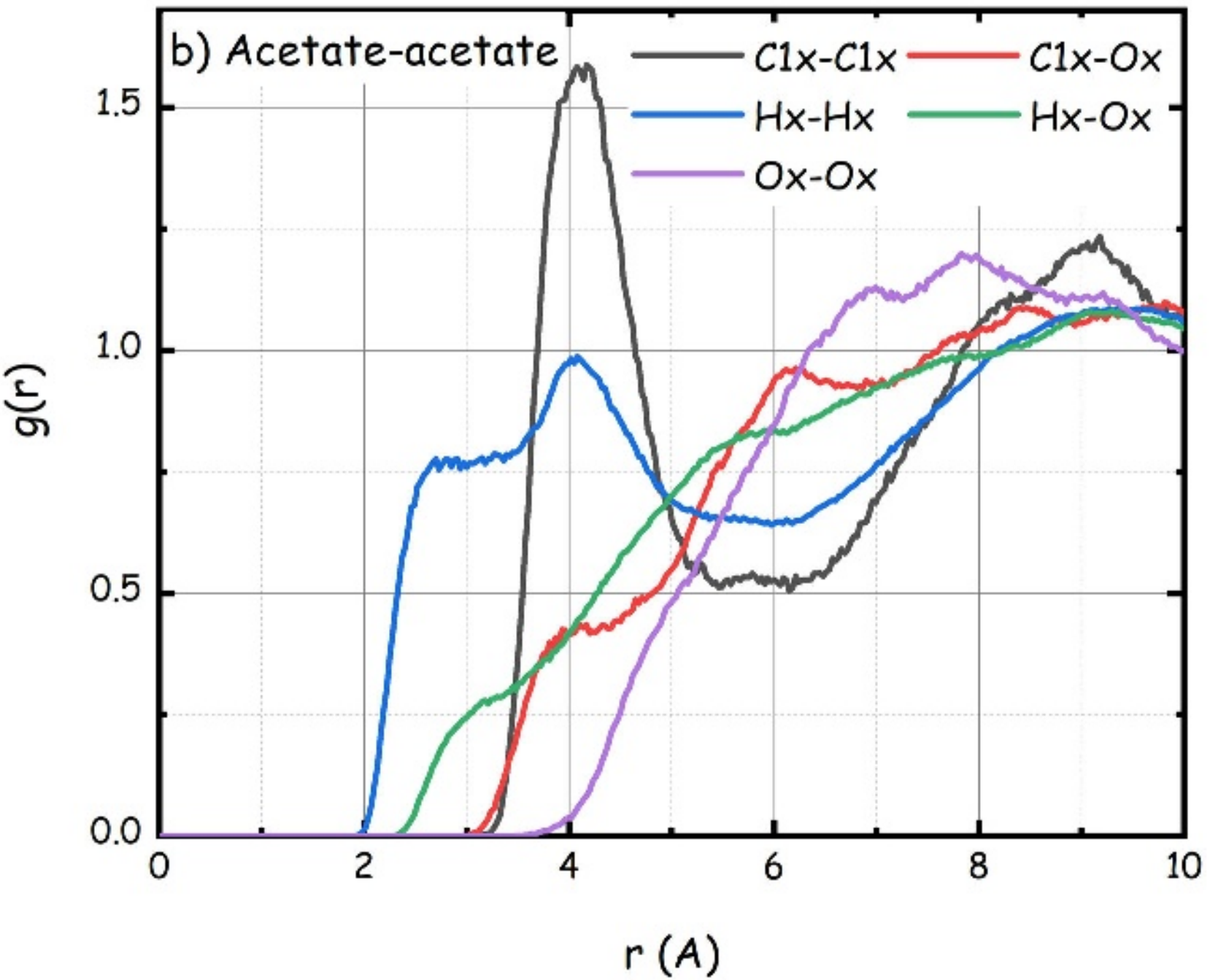
b) Acetate-acetate
C1x-C1x
C1x-Ox
Hx-Hx
Hx-Ox
Ox-Ox
g(r)
r (A)
0.0
0.5
1.0
1.5
0
2
4
6
8
10

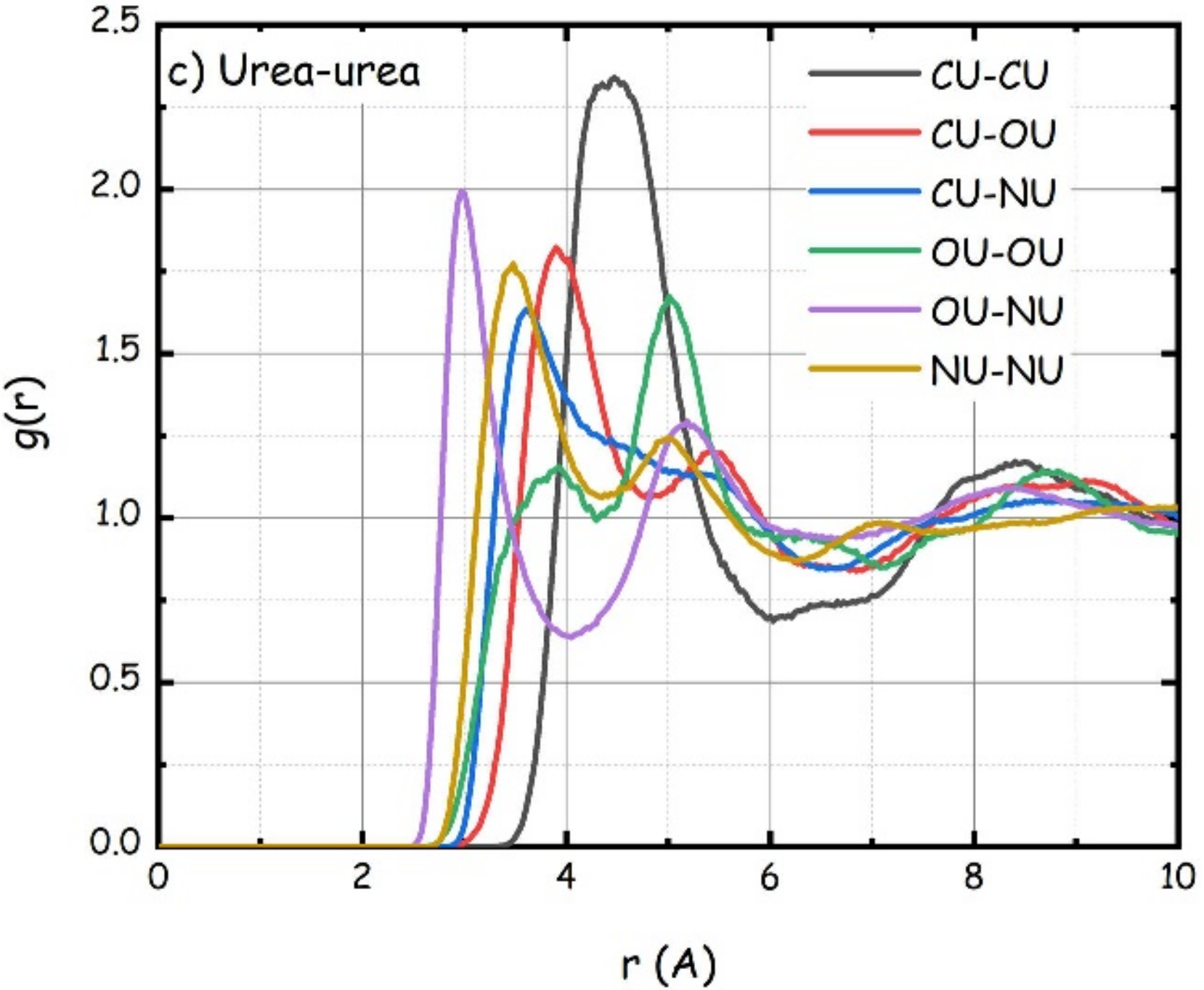
c) Urea-urea
CU-CU
CU-OU
CU-NU
OU-OU
OU-NU
NU-NU
g(r)
r (A)
0.0
0.5
1.0
1.5
2.0
2.5
0
2
4
6
8
10

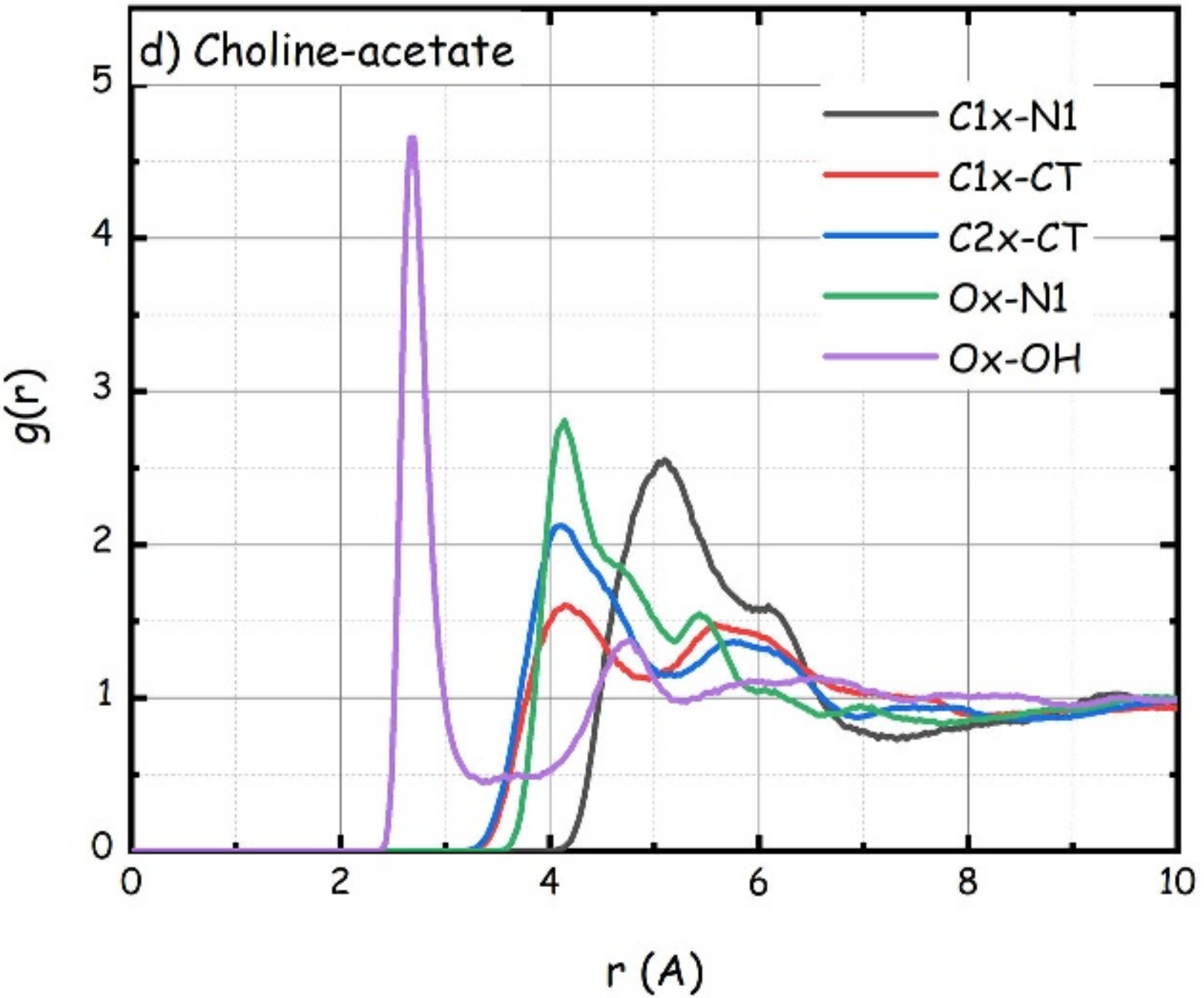
d) Choline-acetate
C1x-N1
C1x-CT
C2x-CT
Ox-N1
Ox-OH
g(r)
r (A)
0
1
2
3
4
5
0
2
4
6
8
10

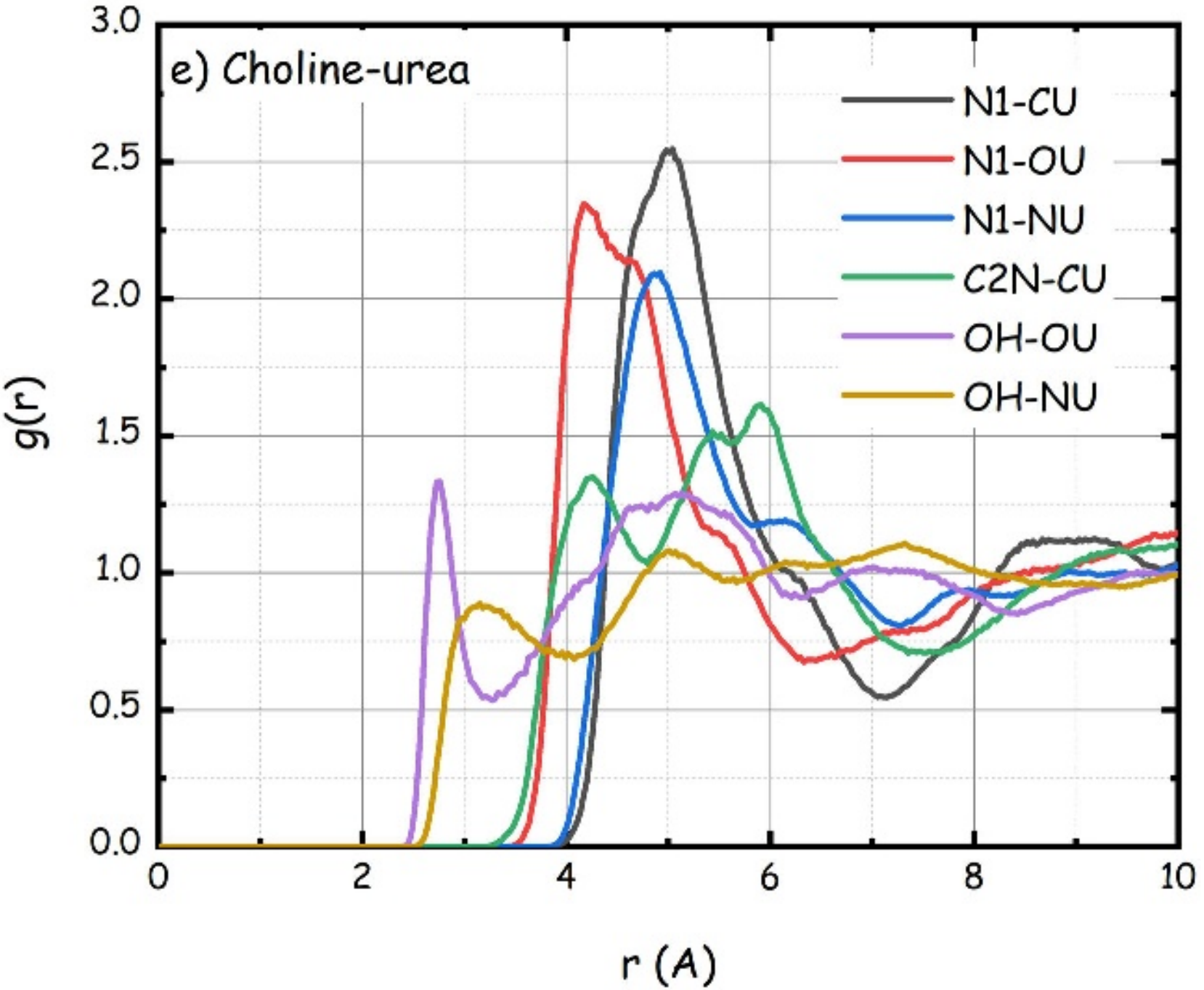
e) Choline-urea
N1-CU
N1-OU
N1-NU
C2N-CU
OH-OU
OH-NU
g(r)
r (A)
3.0
2.5
2.0
1.5
1.0
0.5
0.0
0
2
4
6
8
10

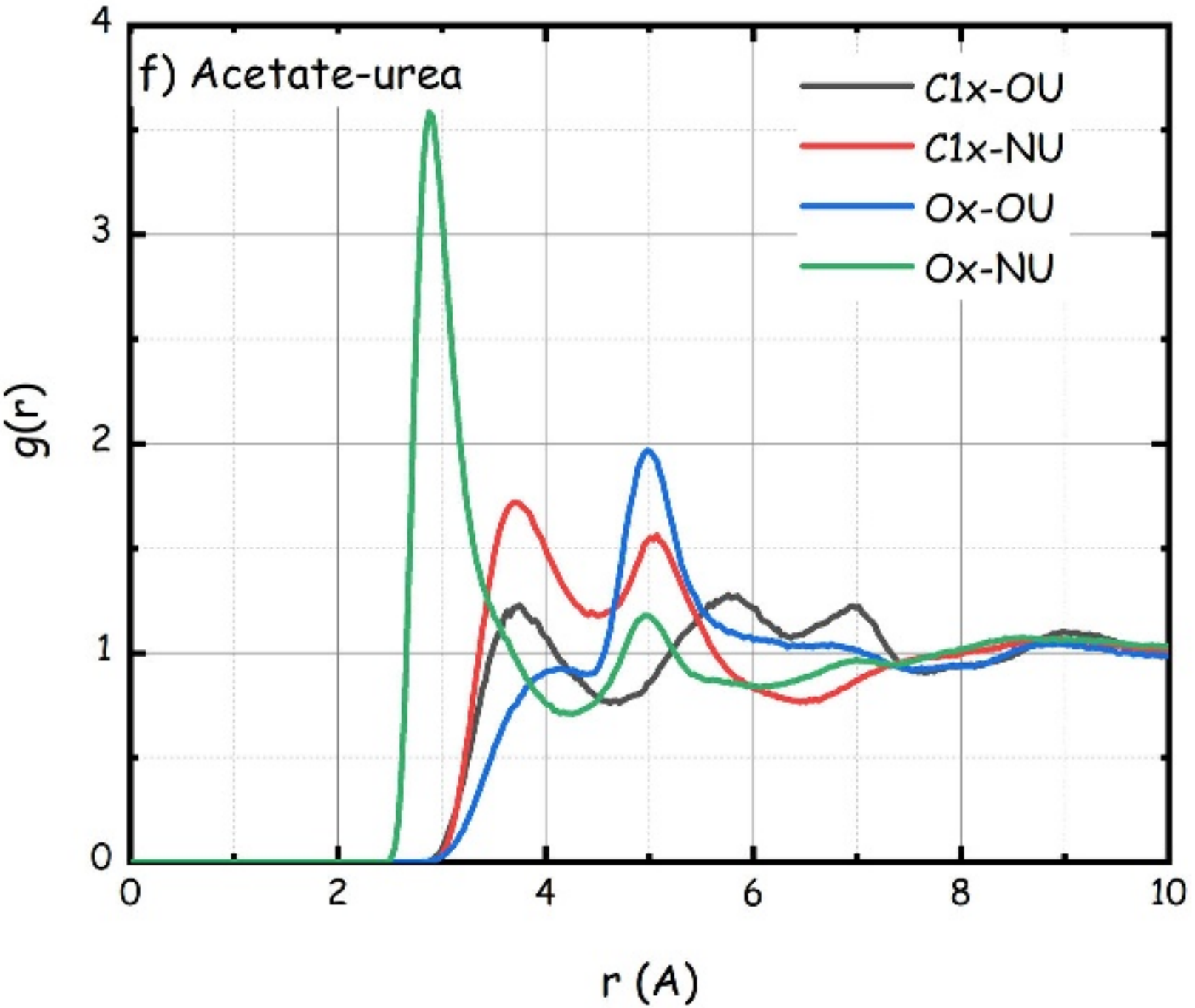
f) Acetate-urea
C1x-OU
C1x-NU
Ox-OU
Ox-NU
g(r)
r (A)
0
1
2
3
4
0
2
4
6
8
10

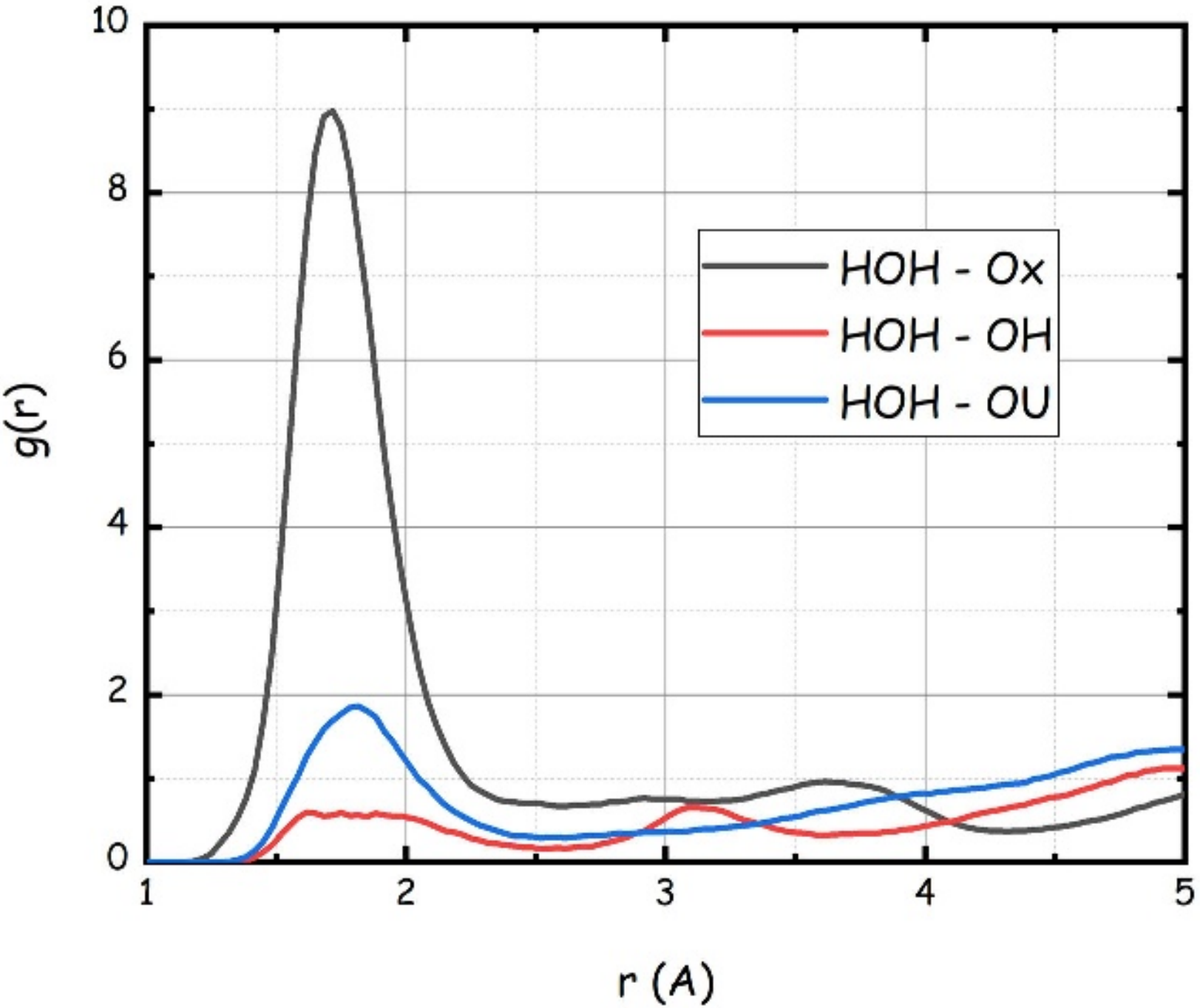
10
8
6
4
2
0
g(r)
1
2
3
4
5
r (A)
HOH - Ox
HOH - OH
HOH - OU

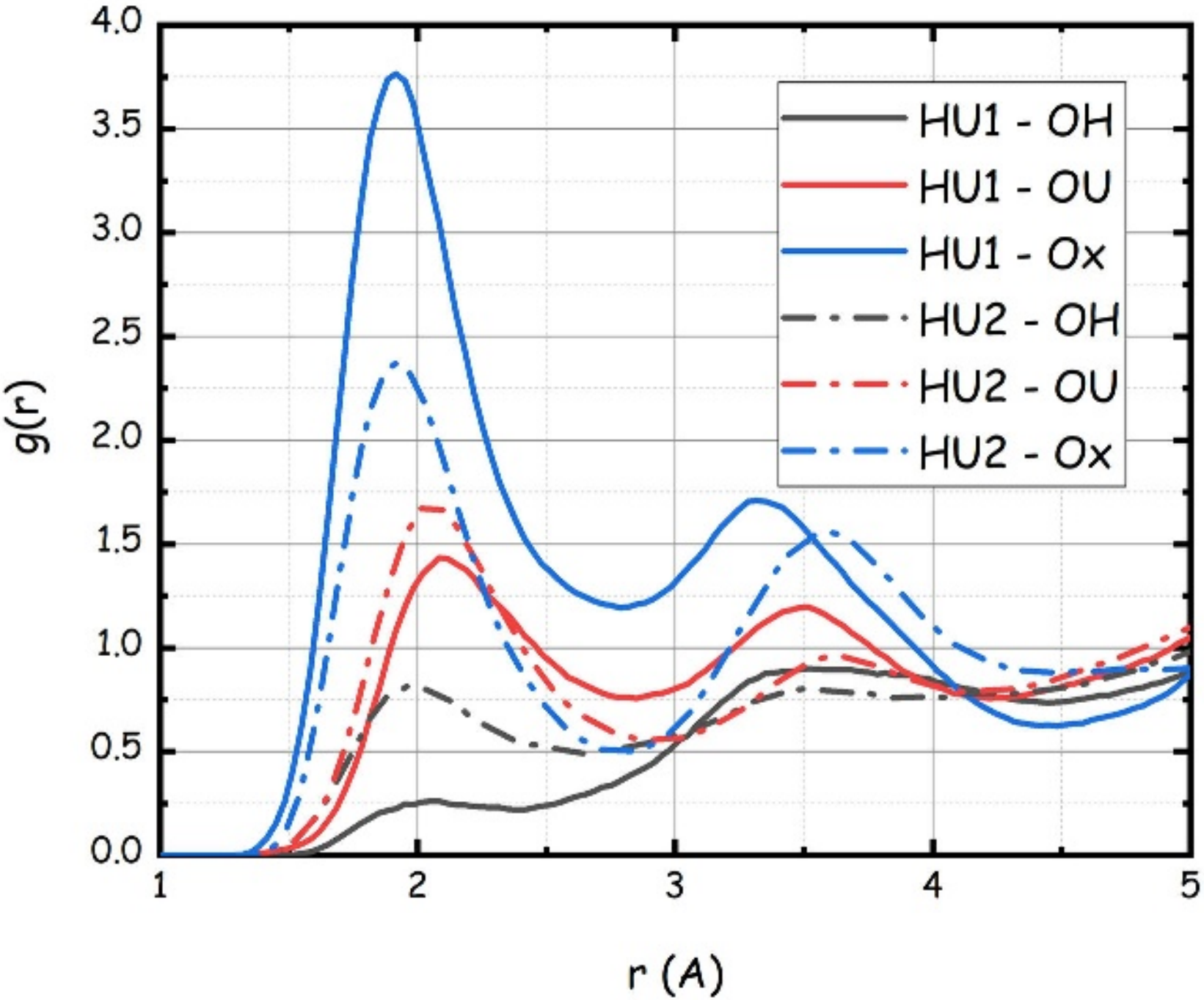
4.0
3.5
3.0
2.5
2.0
1.5
1.0
0.5
0.0
g(r)
1
2
3
4
5
r (A)
HU1 - OH
HU1 - OU
HU1 - Ox
HU2 - OH
HU2 - OU
HU2 - Ox

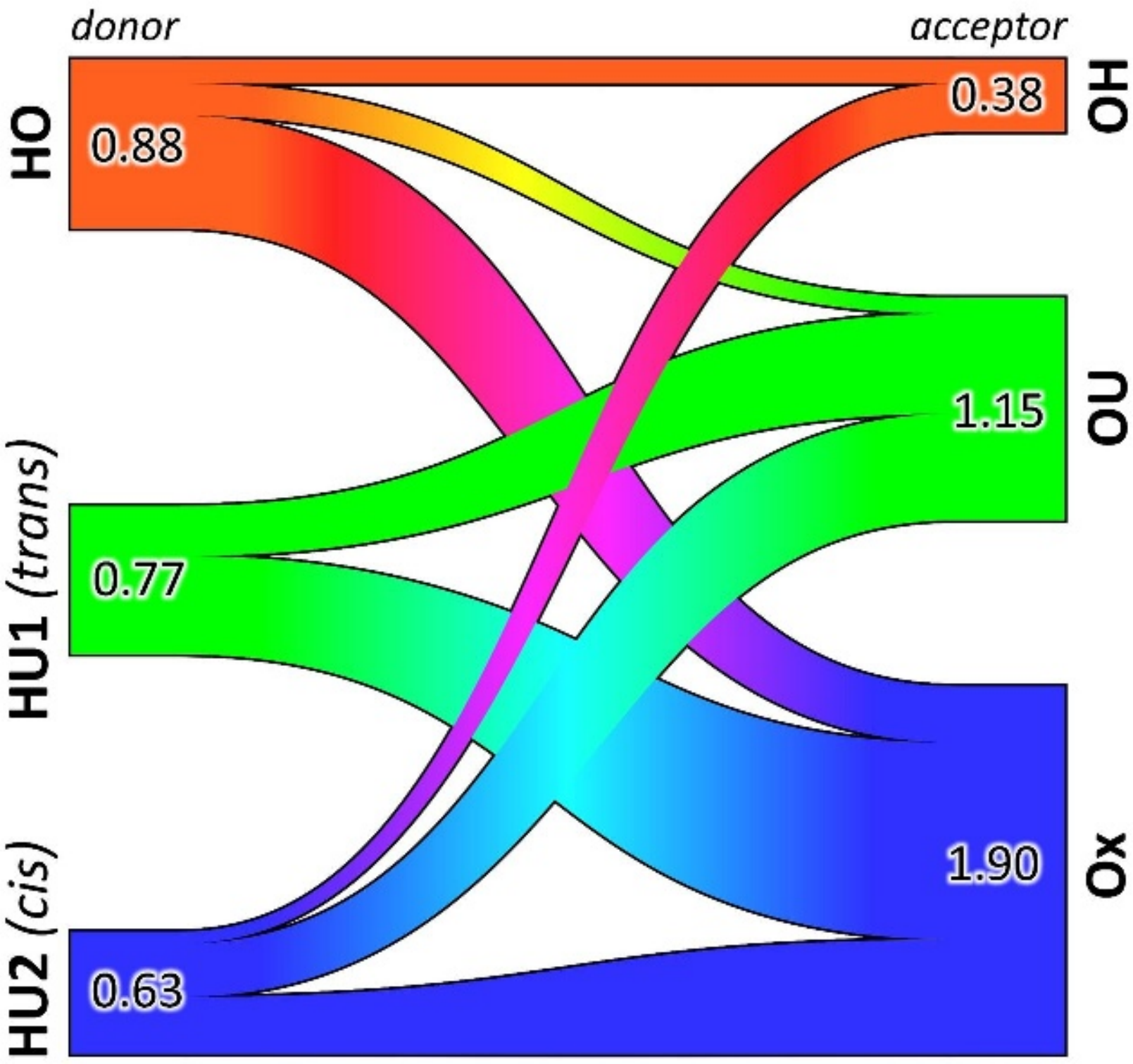
donor
acceptor
HO
HU1 (trans)
HU2 (cis)
OH
OU
Ox
0.88
0.77
0.63
0.38
1.15
1.90

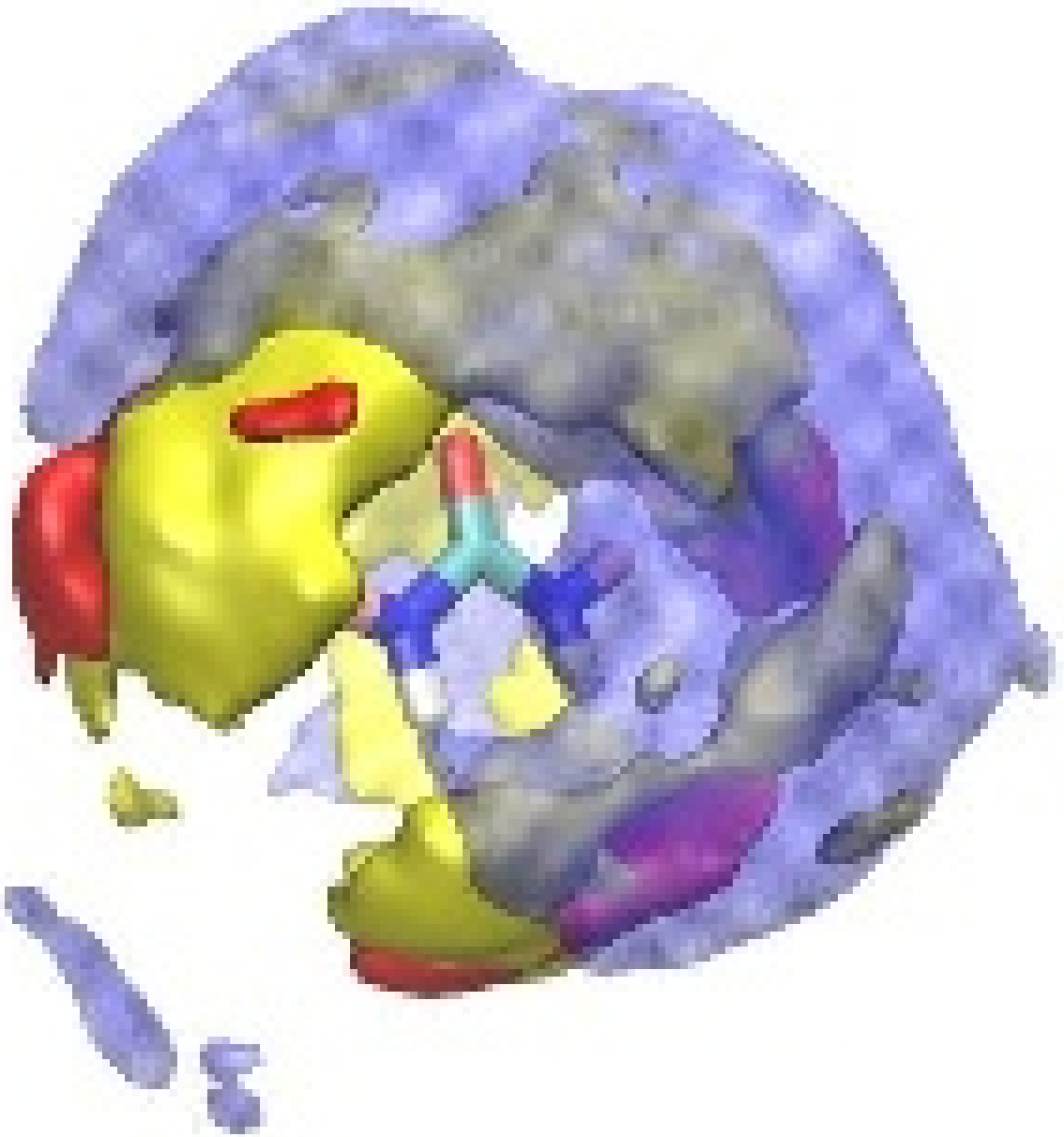

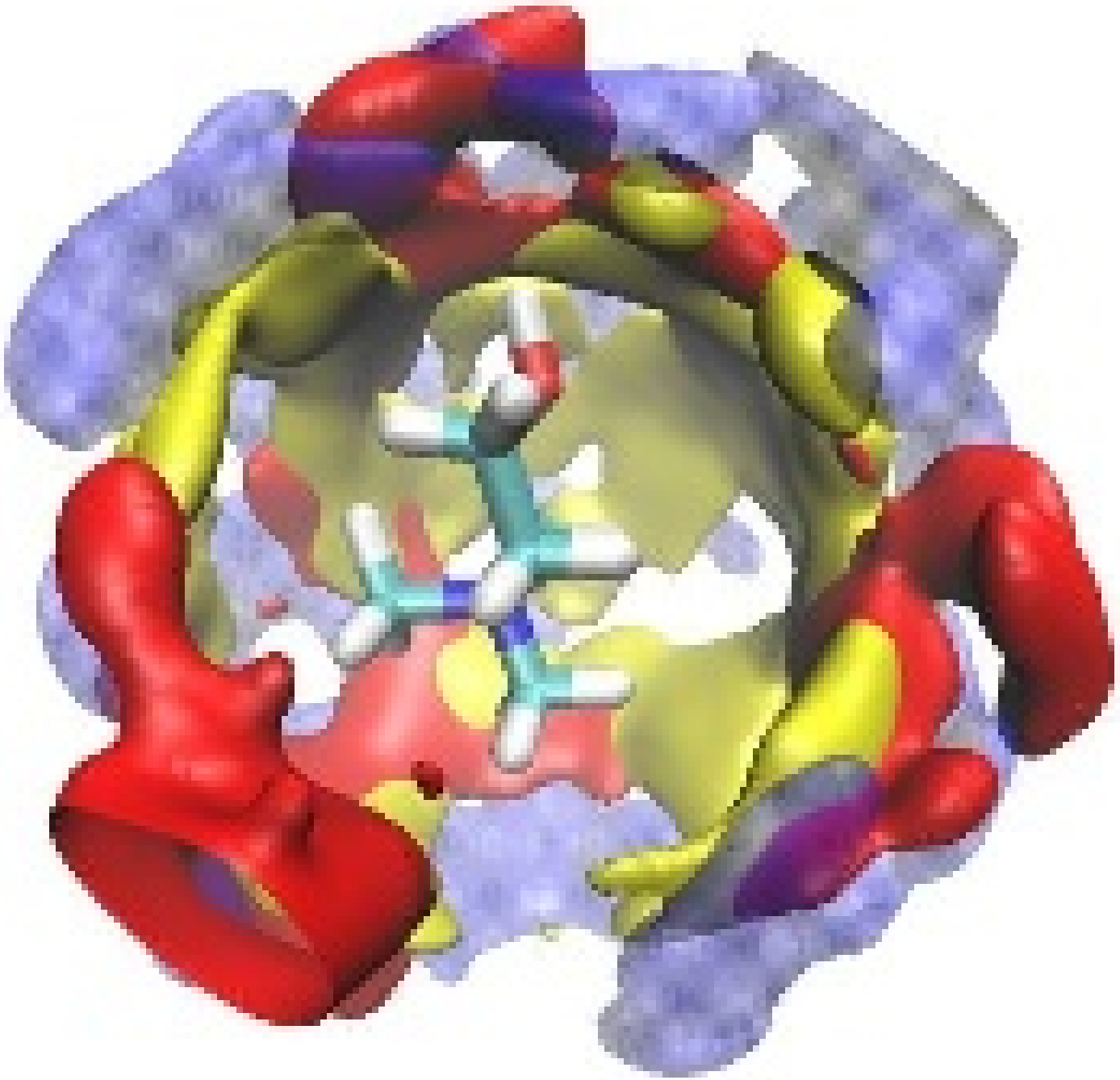

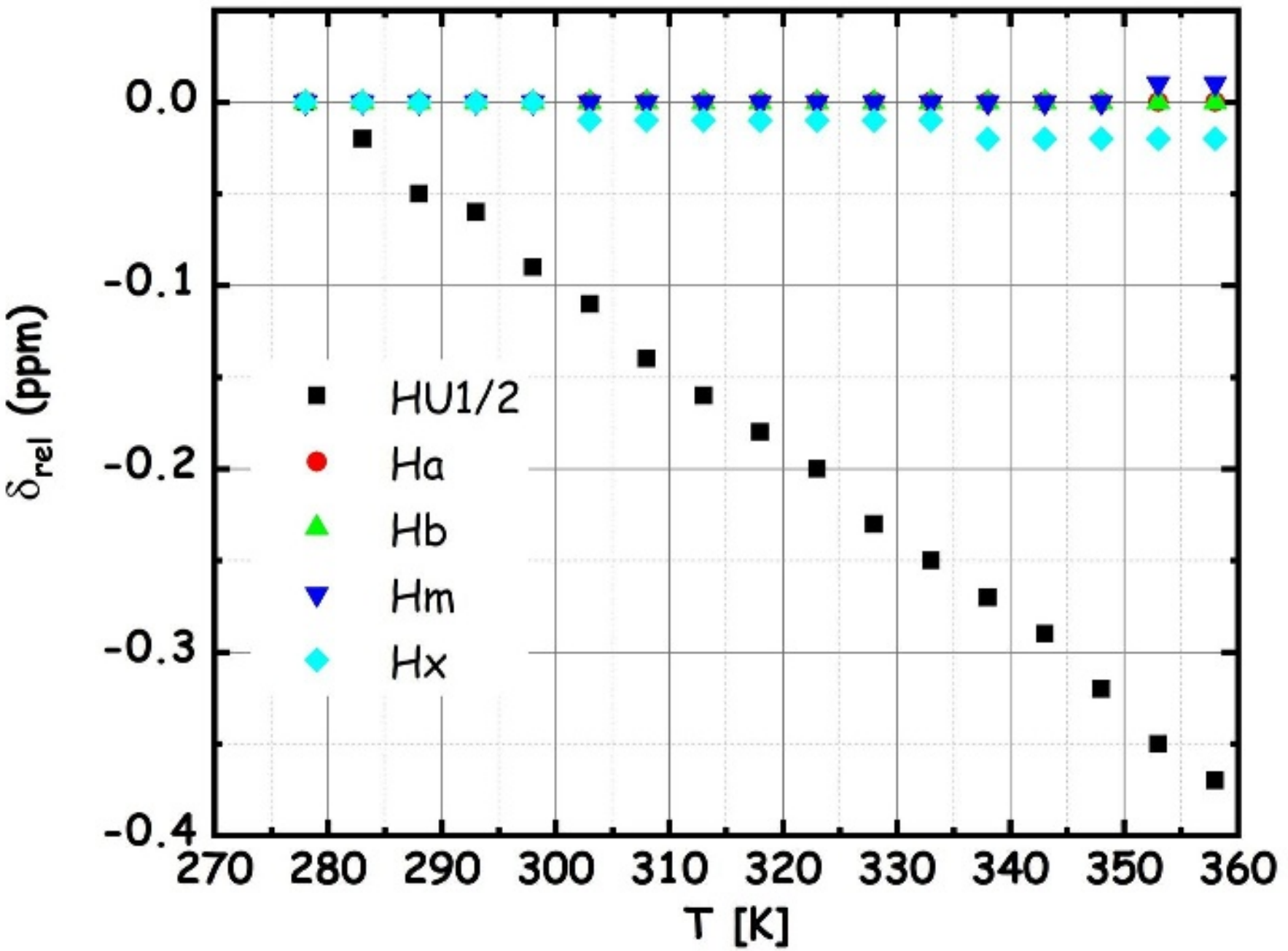
0.0
-0.1
-0.2
-0.3
-0.4
δ_{rel} (ppm)
270
280
290
300
310
320
330
340
350
360
T [K]
HU1/2
Ha
Hb
Hm
Hx

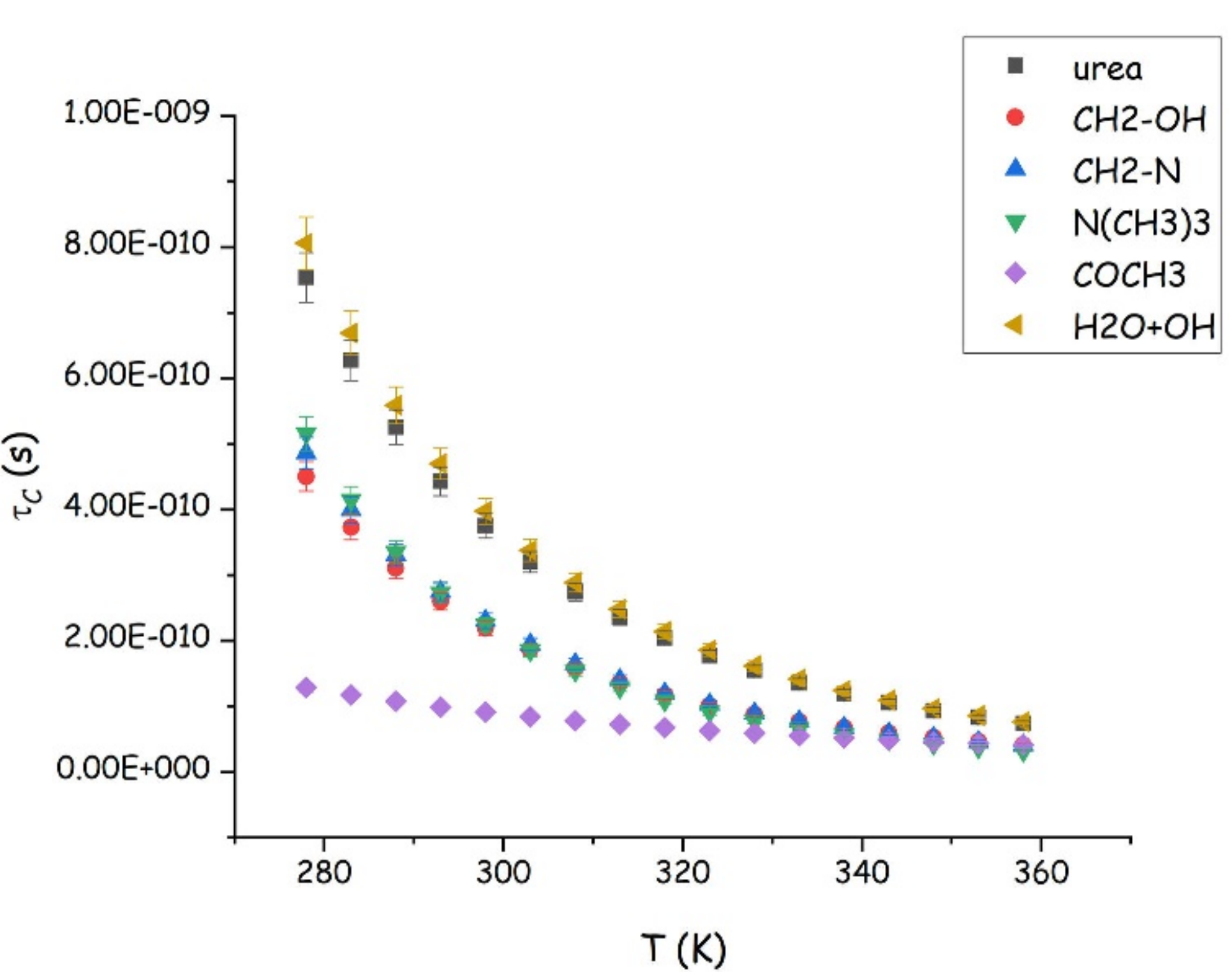
urea
CH2-OH
CH2-N
N(CH3)3
COCH3
H2O+OH
1.00E-009
8.00E-010
6.00E-010
4.00E-010
2.00E-010
0.00E+000
τc (s)
280
300
320
340
360
T (K)

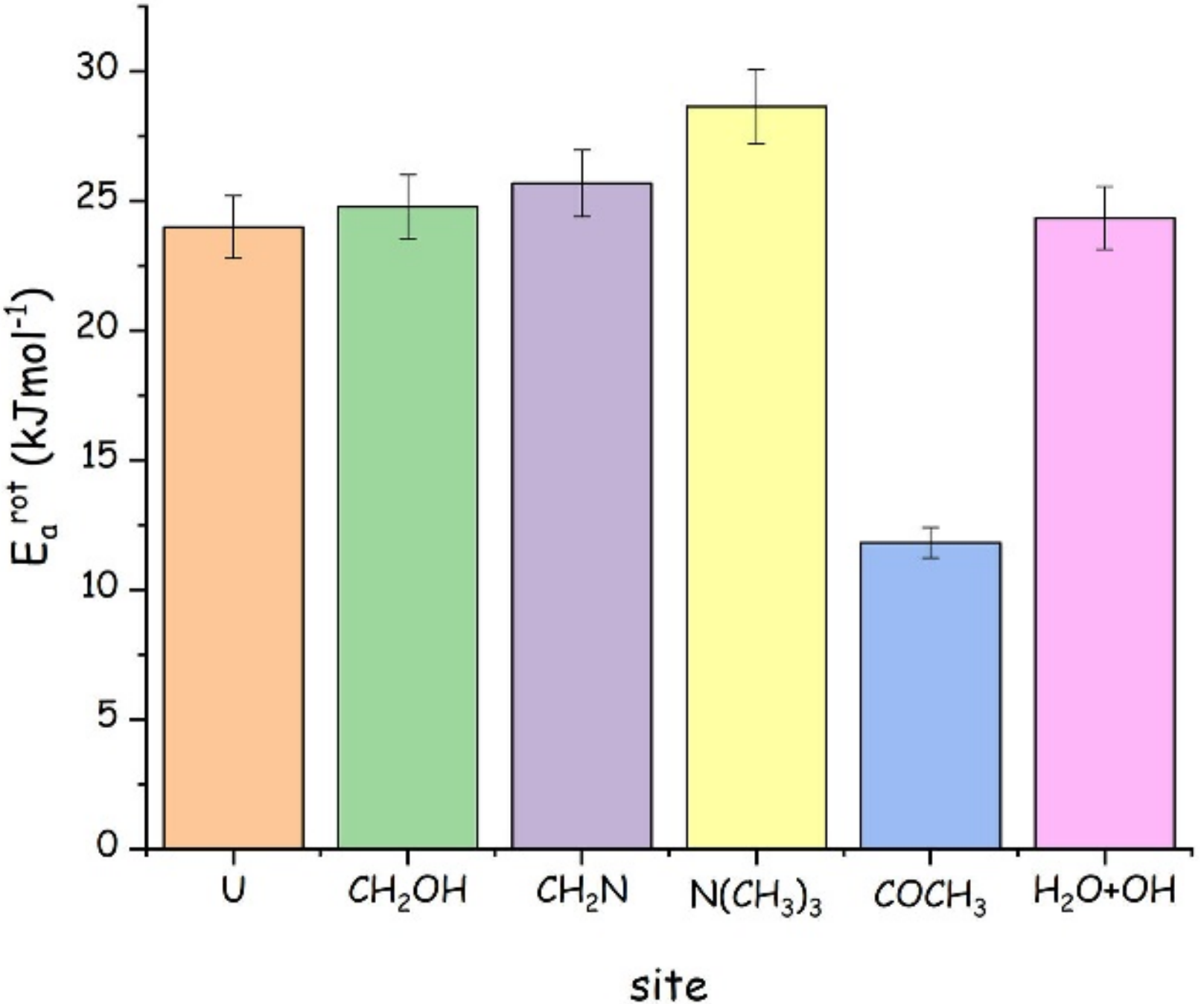
30
25
20
15
10
5
0
E_a^{rot} (kJmol^{-1})
U
CH_2OH
CH_2N
$N(CH_3)_3$
$COCH_3$
H_2O+OH
site

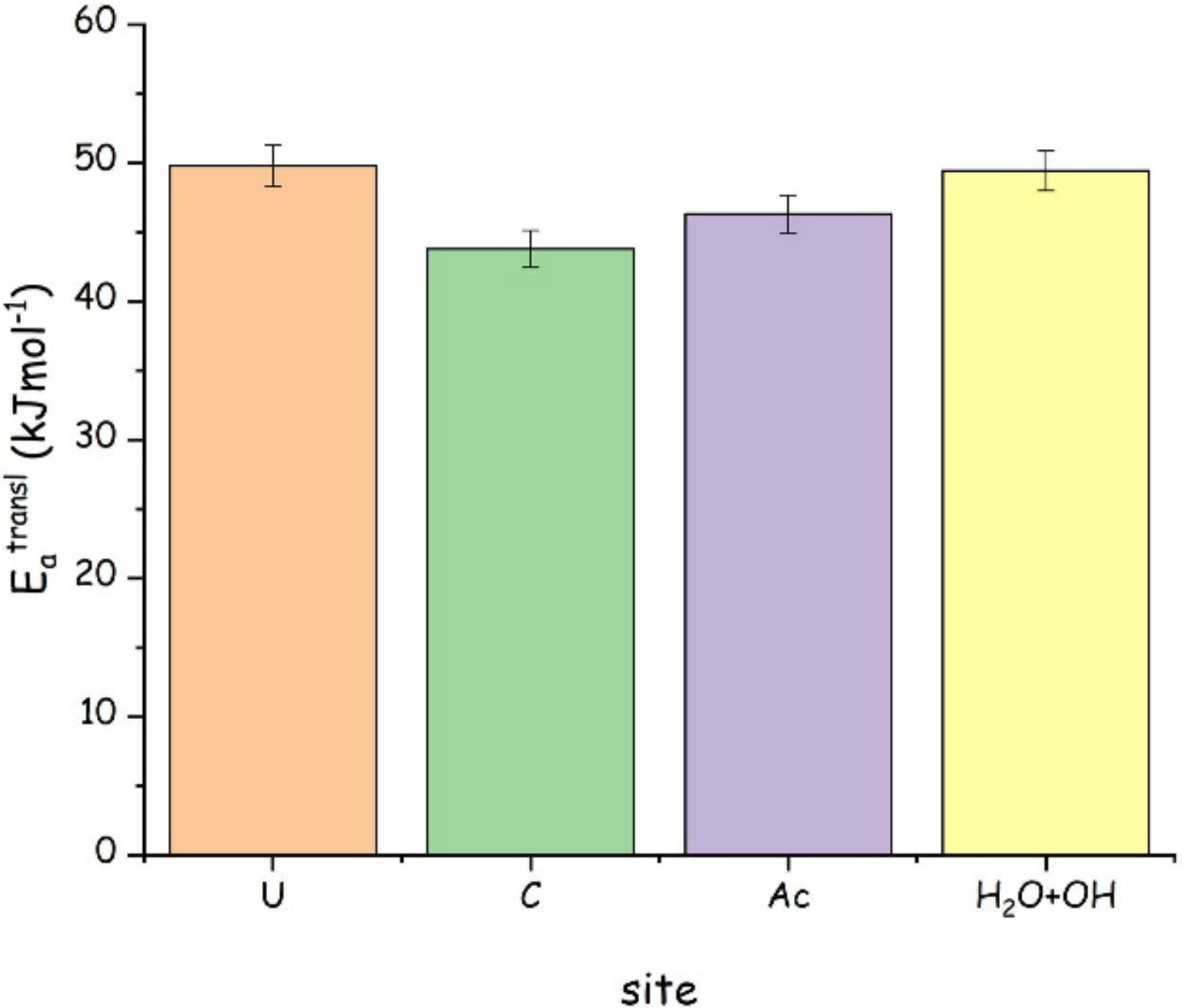
60
50
40
30
20
10
0
E_a^{transl} (kJmol^{-1})
U
C
Ac
H_2O+OH
site